Innovations Deserving
Exploratory Analysis Programs

Highway IDEA Program

Novel Coating Technology for Improving the Corrosion Resistance and Mechanical Properties of Reinforcing Steel in Concrete

Final Report for
Highway IDEA Project 156

Prepared by:
Dr. Leonardo Caseres
Southwest Research Institute

July 2015

TRANSPORTATION RESEARCH BOARD
OF THE NATIONAL ACADEMIES

Innovations Deserving Exploratory Analysis (IDEA) Programs Managed by the Transportation Research Board

This IDEA project was funded by the NCHRP IDEA Program. The TRB

currently manages the following three IDEA programs:

- The NCHRP IDEA Program, which focuses on advances in the design, construction, and maintenance of highway systems, is funded by American Association of State Highway and Transportation Officials (AASHTO) as part of the National Cooperative Highway Research Program (NCHRP).
- The Safety IDEA Program currently focuses on innovative approaches for improving railroad safety or performance. The program is currently funded by the Federal Railroad Administration (FRA). The program was previously jointly funded by the Federal Motor Carrier Safety Administration (FMCSA) and the FRA.
- The Transit IDEA Program, which supports development and testing of innovative concepts and methods for advancing transit practice, is funded by the Federal Transit Administration (FTA) as part of the Transit Cooperative Research Program (TCRP).

Management of the three IDEA programs is coordinated to promote the development and testing of innovative concepts, methods, and technologies.

For information on the IDEA programs, check the IDEA website (www.trb.org/idea). For questions, contact the IDEA programs office by telephone at (202) 334-3310.

IDEA Programs Transportation Research
Board 500 Fifth Street, NW Washington,
DC 20001

Novel Coating Technology for Improving the Corrosion Resistance and Mechanical Properties of Reinforcing Steel in Concrete

IDEA Program Final Report

Contract Number: NCHRP-156

Prepared for the IDEA Program

Transportation Research Board

The National Academies

Principal Investigator: Dr. Leonardo Caseres

Southwest Research Institute® (SwRI®)

April 29, 2014

Table of Contents

EXECUTIVE SUMMARY

The concept of this study was to develop an innovative coating technology with improved corrosion and mechanical performance as compared to existing commercially available coatings used for reinforcing steels. The overall purpose to develop these innovative coatings is to extend the service life of steel and concrete structure, while reducing maintenance costs and improving the reliability and safety of highway structures.

Southwest Research Institute® (SwRI®) is currently advancing an atmospheric solution-based processing technology for fabricating solution-based diamond-like carbon (s-DLC) coatings with the purpose of reducing coating application costs and increasing coating thickness. This s-DLC synthesis process is drastically different than traditional techniques in that it does not require high temperature or vacuum conditions. The proposed atmospheric pressure, low temperature, solution-based processing route opens doors for many applications of DLC films (e.g., protective coatings, friction reduction, corrosion resistance) with substrates previously impractical due to their size, geometry, or incompatibility with vacuum processes.

The s-DLC coating was investigated as a potential coating technique that could be applied to reinforced steels in concrete. Initial steps in this program were to optimize the coating performance prior to the application to reinforced steels. For coating optimization, scanning electron microscopy (SEM), Raman spectroscopy, and electrochemical techniques (e.g., electrochemical impedance spectroscopy and linear polarization resistance) were used to characterize the coating applied to flat steel coupons. After coating optimization, several coated bars were embedded in mortar samples casted with various admixed chloride concentrations (from 0 to 5% wt. of mortar). These mortar samples were partially immersed in simulated seawater for up to 140 days. For comparison purposes, additional reinforcing steel samples were vacuum-deposited with DLC coatings such as standard DLC, multi-layer Si DLC, Si-F-O DLC, and thick DLC coatings. These samples were also prepared in mortar and tested in a similar way as the s-DLC.

Initially in this investigation, SEM analysis revealed an unanticipated problem of cracking in the s-DLC films deposited on the rebar surface. SwRI investigated methods to mitigate this cracking, including altering the parameters in the pyrolysis step. These alterations included changes to the heating and cooling rates and exploring alternative wet-coating techniques. Multiple layers of s-DLC films were also applied to the rebars in efforts to mitigate cracking. Both approaches were successful in mitigating the formation of cracks.

The corrosion properties of the coated mortar samples were examined using linear polarization technique. The linear polarization results showed that for the case of 0% chloride content, corrosion rates were negligible/low (<0.1 mpy) for the s-DLC, Si-F-O DLC, and thick DLC coatings. For the standard DLC and multi-layer Si DLC coatings, corrosion rates were moderate (0.65–0.90 mpy). As expected, as the chloride concentration was increased, corrosion rates also increased. This increase was more notable for the s-DLC coating. By the end of the 140-day exposure, the corrosion rate for 0.5% chloride concentration was high (1.9 mpy) for the s-DLC coating, moderate (0.55 mpy) for the standard DLC and multi-layer Si DLC coatings, and negligible (<0.07 mpy) for the Si-F-O DLC and thick DLC coatings. This indicates that coating defects are likely to be present in the s-DLC, standard DLC, and multi-layer Si DLC coatings. Similar trends were recorded for the 1% and 3% chloride contents. For the 5% chloride concentration, all of the DLC coatings, except for the thick DLC coating, showed high corrosion rates (>1.4 mpy), whereas the thick DLC coating displayed a moderate corrosion rate (0.75 mpy). The linear polarization results were in agreement with the EIS measurements. As reported by others, polarization resistance values of epoxy-coated rebars in chloride-contaminated concretes can be as low as 20 kohm. This value is about one order of magnitude larger than the polarization results of the DLC coatings obtained in this investigation.

Future research is needed to improve the s-DLC coating properties so that it may be usable as a cost-effective protective coating for reinforcing steel in concrete. While the mechanical properties of the s-DLC coating are excellent, its corrosion protective performance is still lacking. Once this is corrosion performance is improved, SwRI will formalize teaming arrangements through negotiated business agreements to support technology integration and transition. SwRI has already engaged in discussions with small businesses regarding scale-up synthesis from the pilot synthesis to larger production (500–2,000 gallons) of s-DLC coatings.

SIGNIFICANCE OF THE PROBLEM

Carbon steel bars (rebars) embedded in concrete are subject to extensive damage due to corrosion, especially those located in the northern states and coastal areas in the United States. Early in the life of reinforced steel concretes, the rebars are protected from corrosion by the alkaline nature of the surrounding concrete matrix. However, chloride ions from seawater and deicing salts accumulate on the surface of the concrete and slowly migrate through the concrete cover to the underlying steel. When the chloride concentration at the rebar depth exceeds a critical threshold value, the protective passive layer on the steel surface breaks down and active steel corrosion begins with formation of corrosion products at the rebar surface (*1*). The corrosion products occupy a volume that can be several times larger than that of the bare steel, thus causing cracks and spalls of the concrete cover, decreasing the rebar diameter, and decreasing the steel/concrete bond strength (*2*).

To extend the service life of concrete structures, several transportation agencies employed epoxy-coated rebars (ECR) in the late 1970s. ECR was incorporated as a corrosion protection measure for service in environments that were considered extremely aggressive for bare carbon steel applications. However, varying corrosion performance has been reported in field and laboratory examinations (*3, 4*). ECR has been primarily used with success in bridge decks exposed intermittently to deicing salts. In contrast, poor corrosion performance as well as loss of adhesion bond between the ECR and the underlying steel rebar has been observed in structures with ECR exposed to marine environments, where severe structural corrosion and coating disbondment developed after only a few years in service. As a result, it is evident that the use of ECR does not always prevent corrosion, especially in aggressive environments.

New methods intended to improve corrosion durability of ECR; for example, the dual polymer-zinc coating, are being explored (*5*). The dual coating contains a 0.002 in. (0.05 mm) thick layer of nearly pure zinc, applied by thermal spraying to the steel surface, covered by a secondary 0.008 in. (0.2 mm) thick epoxy polymer layer. Preliminary results (*6*) have shown that the dual polymer-zinc coating experienced severe corrosion under strong anodic polarization in simulated pore solution admixed with chlorides, but the extent of corrosion was significantly less than for ECR.

Other types of coatings such as stainless steel-clad rebars and galvanized steel rebars have also been examined for potential carbon steel replacement. Despite the acceptable galvanic protection of the galvanized coating to the underlying steel, the galvanized coating dissolves quite rapidly when exposed to high pH environments. In addition, at those high pH values there is a production of H_2 gas at the rebar/concrete interface, which causes a decrease in bond strength. In contrast, the stainless steel clad rebars offers excellent corrosion resistance protection when the clad surface is unblemished, but are 2–3 times more expensive than unclad rebars. For clad rebars containing coating breaks, limited cathodic protection to steel has been recorded (*7*). Other coatings and materials (e.g., duplex stainless steels) have been explored, but their high cost-benefit ratio makes them unsuitable. As a result, more affordable and enhanced long-term corrosion performance coatings must be developed in order to improve the reinforcing steel durability by extending the length of time until the initiation stage of corrosion.

The overall focus of the proposed research was to provide the transportation agencies with a cost-effective coating technology that shows improved corrosion and mechanical performance compared to existing coatings used for steel with the purpose of reducing maintenance costs and improving the durability, reliability, and safety of highway structures. The approach described in this report is to use s-DLC coatings as an alternative to the current coatings being used. The technical objectives of the program were to: (1) develop and optimize an inexpensive atmospheric solution-based processing technology by which s-DLC coatings can be deposited on carbon steel commonly used for reinforced steel concrete applications, and (2) investigate the electrochemical and mechanical properties of these s-DLC coatings exposed to solutions with compositions bracketing those encountered in concrete, focusing mainly on marine environment applications.

BACKGROUND

Solution-Based Diamond-Like Carbon (S-DLC) Coatings

Due to their excellent mechanical and tribological properties, diamond-like carbon (DLC) coatings are widely used as protective overcoats in various industries. DLC is defined as amorphous carbon with a significant fraction of sp^3 bonds. The designation diamond-like arose because the material is characterized by properties that are, to a certain extent, similar to those of diamond: high hardness, chemical inertness, high electrical resistance and optical transparency in the visible and infrared. DLC coatings are typically prepared by vacuum deposition processes such as plasma-enhanced chemical vapor deposition (PECVD), ion beam assisted deposition (IBAD), and magnetron sputtering. These vacuum deposition processes have the limitations of (i) high costs, (ii) slow rates of film formation, (iii) limited total film thickness, (iv) limited part sizes based on the volume of the vacuum chamber, (v) restricted to vacuum-compatible substrates, and (vi) inability to combine with reinforcing materials.

SwRI® is currently advancing an atmospheric solution-based processing technology for fabricating solution-based diamond-like carbon (s-DLC) coatings that addresses these limitations. This method utilizes chemical synthesis of hydrocarbon polymers possessing diamond-like structure at the atomic level and subsequent pyrolysis and potentially photolysis to convert the polymers to diamond-like carbon. This s-DLC synthesis process is drastically different than traditional techniques in that it does not require high temperature or vacuum conditions. The proposed atmospheric pressure, low temperature, solution-based processing route opens doors for many applications of DLC films (e.g., protective coatings, friction reduction, and corrosion resistance) with substrates previously impractical due to their size, geometry, or incompatibility with vacuum processes.

The properties of DLC are typically determined by composition represented by a ternary phase diagram for sp^2, sp^3 and H content (Figure 1). The composition of the s-DLC is determined by the chemistry of the precursor organic molecules. In recent years, different synthesis methods of carbon polymers possessing diamond-like structure at the atomic level have been reported (*8, 9*). The majority of these polymers are classified as polycarbynes, in which poly(phenylcarbyne) and poly(hydridocarbyne) have been the main focus. Polycarbynes $(CR)_n$ have a continuous random network backbone of tetrahedrally hybridized C atoms bound by σ-bonds to three other C atoms and one substituent. The original synthesis of polycarbynes (*10*) required inert atmosphere processing with dangerous alkali metals, a difficult and potentially expensive process (*8, 10*). SwRI has expanded on these previously reported studies by investigating variations of liquid/solid two-phase condensation polymerization reactions of various hydrocarbon monomers in the presence of solid potassium hydroxide or sodium hydroxide particles at room temperature and atmospheric conditions as a synthetic route for polymers possessing diamond-like structure similar to polycarbynes. Compared to previous reported methods, this synthetic process is much more flexible, inexpensive, and scalable for manufacturing.

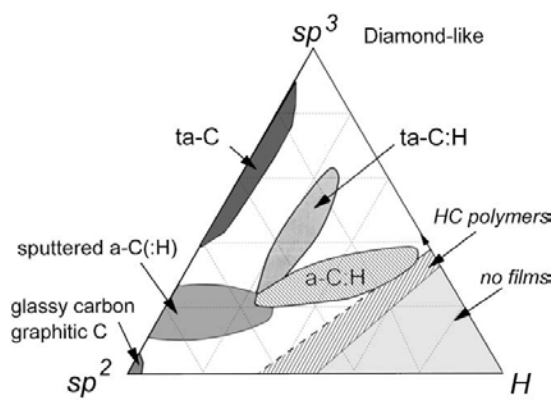

FIGURE 1 Ternary phase diagram of amorphous carbons. The three corners correspond to diamond, graphite, and hydrocarbons.

Other Types of Diamond-Like Carbon Coatings

Plasma ion immersion deposition (PIID) technique is another method used to deposit hard DLC coatings (Figure 2). For the PIID process, parts are placed in a vacuum chamber. When the chamber is pumped down to a low pressure (~10^{-6} Torr), a gas is fed into the chamber to typically about 10 to 15 mTorr. A pulsed train of negative voltage is applied to the parts and a pulsed-glow discharge plasma is generated in the vacuum chamber. Because the parts are pulsed, the voltage also draws the ions to the part's surfaces. Depending on the ion species (precursor gases), either ion sputter cleaning (if argon is used) or deposition of DLC can be performed (if a carbonaceous gas such as acetylene is used). Typically, to ensure good adhesion of the coating, components are sputter-cleaned with argon first. Then, without breaking vacuum or interrupting the discharge, deposition can proceed by gradually reducing the argon flow and

increasing the acetylene flow to form the desirable DLC coating. Further bonding improvement of DLC coating onto ferrous materials can be made by depositing an adherent bond layer such as silicon, silicon carbide, or silicon nitride, using various silicon-containing precursors before the DLC deposition.

The DLC films produced by the PIID method have an amorphous structure with a high hardness as well as high chemical inertness (Figure 3). The electrochemical corrosion behavior (*11–13*) and erosion performance (*14*) of DLC films in various aggressive environments have been studied. A thin DLC film from several nanometers to a few micrometers can prevent the metallic substrate from corrosion attack (*11*, *15*). The DLC films prepared by the PIID method have low friction (*16*) and are hydrophobic (*17*) with a water contact angle of up to 140°.

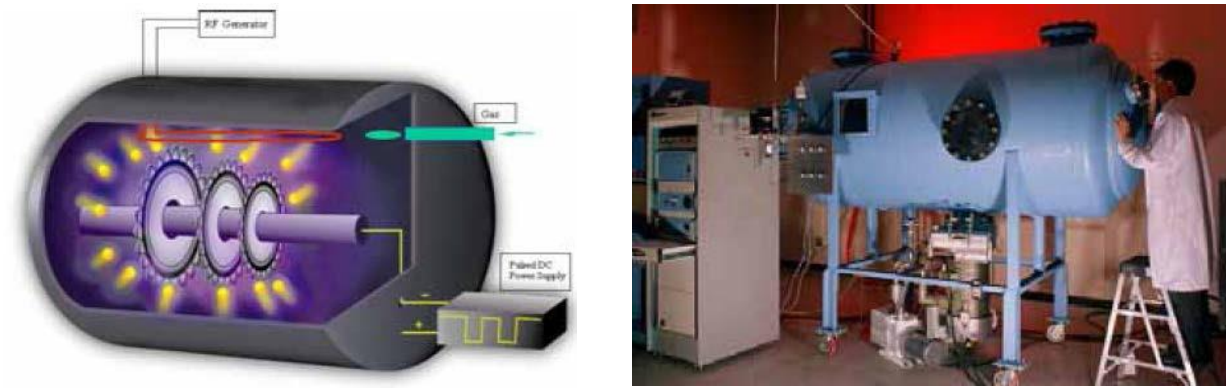

FIGURE 2 Plasma immersion ion deposition (PIID).

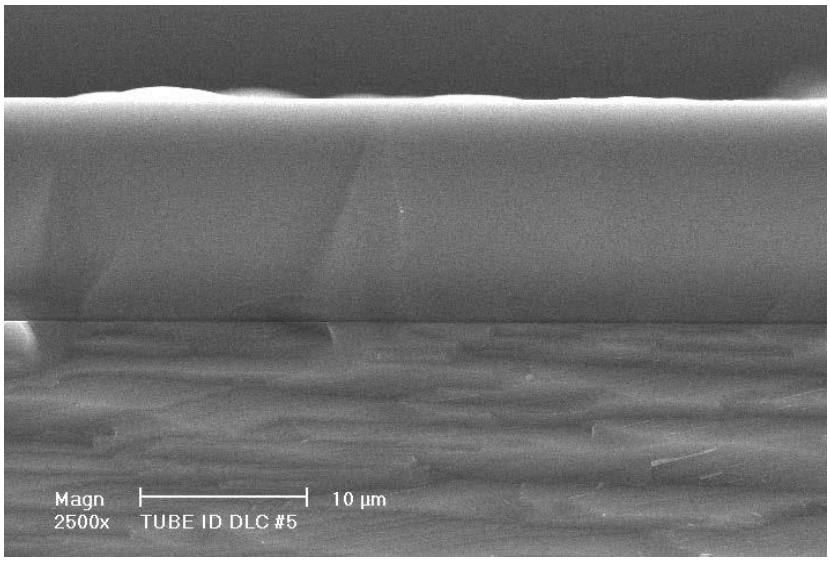

FIGURE 3 Cross-sectional SEM image of a DLC coating.

EXPERIMENTAL APPROACH

The work plan was divided into three main technical tasks. Task 1 addressed the coating application, characterization, optimization, and mechanical evaluation. Task 2 dealt with the coating performance assessment via electrochemical evaluation. Tasks 1 and 2 were performed using coated flat coupons and carbon steel rebars. The flat coupons coated with SwRI-developed s-DLC coating were used to characterize and optimize the coating application technique, chemistry, adhesion, and uniformity by using Raman spectroscopy, and scanning electron microscopy (SEM). The coating characterization and optimization was conducted by performing mechanical tests including the hardness, Young's modulus, wear, and adhesion and by immersing the coated coupons in simulated pore water solutions with varying chloride concentrations at room temperature and atmospheric pressure. After coating optimization, reinforcing steel bars embedded in mortars were used for further testing. As part of Task 2, additional DLC coatings, prepared by the PIID method described above, were also evaluated and the results were compared to the s-DLC coatings.

COATING PREPARATION

The s-DLC Coating

SwRI developed a synthetic procedure consistent in yielding DLC polymer precursor product with reproducible chemical properties by reduction of α-α-α-trichlorotoluene in the presence of solid potassium hydroxide particles at room temperature and normal atmospheric conditions. Polymerizations were carried in three-necked flasks that consisted of one condenser, one dropper, and one glass tube for nitrogen bubbling. The flasks were seated on magnetic stirrers. An optimal synthetic procedure was established through systematic variations on the polymerization reaction. The polymer precursors can be converted to s-DLC by a simple heat treatment process in an inert atmosphere or in vacuum. Thermal analysis in argon was done for the raw and purified polymer precursor products. Figures 4 and 5 show the experimental setup and the sequence of the polymerization reaction at various polymerization times.

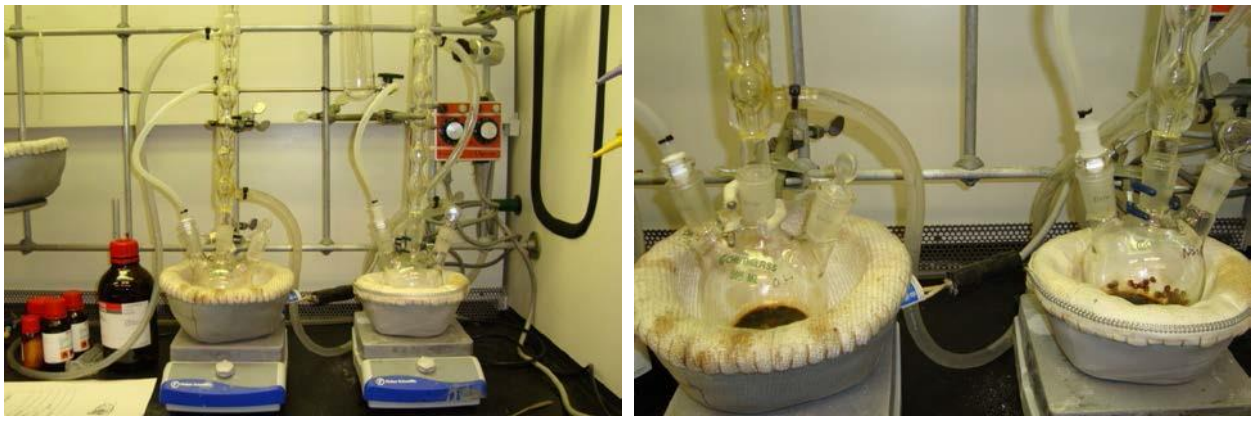

FIGURE 4 Photographs of the experimental setup for chemical synthesis of s-DLC coatings.

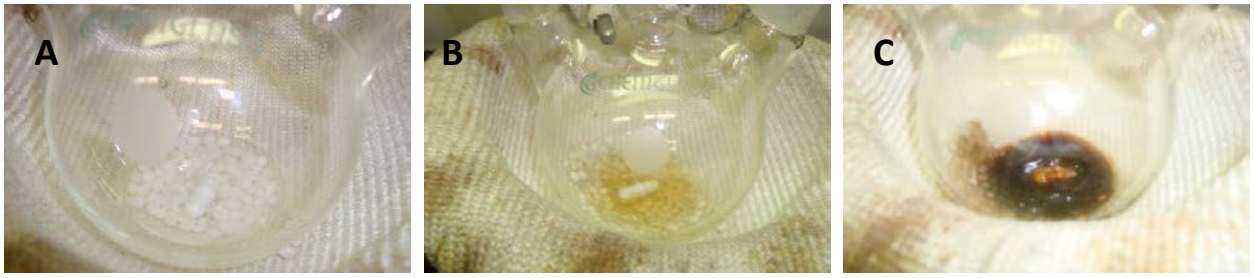

FIGURE 5 Photographs of the polymerization reaction at (a) t = 0 min, (b) t = 10 min, and (c) t = 2 hr.

Following synthesis, polymer solutions were prepared. These polymer solutions were deposited as films using wet coating techniques, such as spray-coating and spin-coating (Figure 6). Spray-coating proved to be the best means to deposit uniform coatings onto metal substrates. Spray-coated polymer thin films were prepared on Si wafer, stainless steel 304 coupons, and carbon steel bars. The coated substrates were subsequently heated at 752°F (400°C) for 2 hours in argon gas to convert the films to s-DLC.

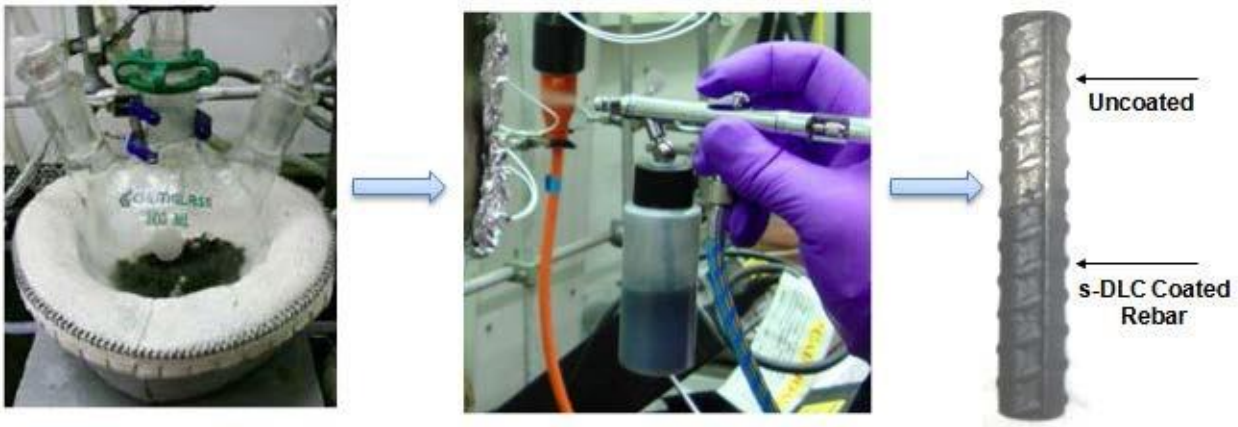

FIGURE 6 Developed atmospheric solution-based processing technology by which DLC coatings can be deposited on rebar samples. Process steps involve chemical synthesis of DLC polymer precursors, spray-coating polymer precursor solutions onto rebar substrates, and subsequent heat treatment to convert the films to s-DLC.

As mentioned earlier, flat coupons, 1 in. by 2 in. by 0.125 in. (2.54 cm by 5.1 cm by 0.3 cm), were used for coating optimization. Figure 7 shows the experimental setup used to test the electrochemical behavior of the s-DLC coating. The test cell consisted of a glass cylinder hosting a platinum counter electrode, a Standard Calomel Reference Electrode (SCE), and the working electrode. The solution used for the coating optimization was simulated concrete pore solution with composition and pH as reported in Table 1. Periodically, powder NaCl was added to the solution to attain chloride concentrations ranging from 0 to 1.5 mol/L. Coating performance was evaluated by performing electrochemical impedance spectroscopy (EIS) and open circuit potential measurements versus time. All the measurements were conducted at room temperature under atmospheric pressure.

As part of the characterization process, the s-DLC coating was examined with SEM, FTIR, and Raman spectroscopy. Additionally, the mechanical properties of the coatings including microhardness, Young's modulus, wear, and adhesion were investigated. Once the coating was optimized and characterized, multiple sections of rebars of size #3 were coated and embedded in mortar samples (Figure 8).

TABLE 1
Composition of the simulated concrete pore solution used to characterize the s-DLC coating

pH	NaOH, g/L	KOH, g/L	$Ca(OH)_2$, g/L
13.3	3.7	10.5	2.0

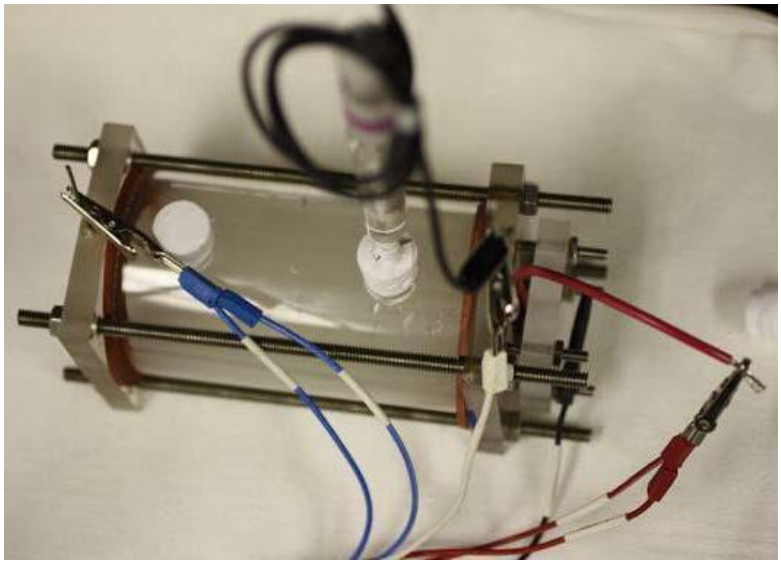

FIGURE 7 Test cell used to characterize the s-DLC coating corrosion properties.

FIGURE 8 Photograph comparing s-DLC coated rebar section to an uncoated rebar section.

The PIID DLC Coating

As mentioned above, additional DLC coatings, prepared by the PIID method described above, were also evaluated. For this coating application, rebars of size #3 and 6 in. (15.2 cm) in length were cleaned ultrasonically in an alcohol bath and then hung in a meshed metal cage inside the PIID vacuum chamber. After pumping down the processing chamber to 10^{-5} Torr, Ar gas was fed into the system so that its pressure reached approximately 15 mTorr. A train of negative pulsed voltage was then applied to the meshed cage as well as the samples at 4 kV with the pulse frequency of 1,000 Hz and pulse width of 20 µs to generate the plasma similar to that in hollow cathode discharge. The samples were first sputter cleaned with Ar ions for 30 min; then trimethylsilane [TMS, $(CH_3)_3SiH$] was introduced into the processing chamber to deposit a SiC bond (adhesion) layer. This process duration was 20 minutes. After that, acetylene (C_2H_2) was introduced into the vacuum chamber to deposit a layer of amorphous carbon DLC, which lasted for 20 min. Then another layer of SiC was deposited using the TMS gas for 10 minutes, followed by another DLC layer using C_2H_2 gas for 20 minutes, and another layer of SiC. Finally, DLC was deposited for 1 hour. In this way a multi-layered DLC consisting SiC/DLC/SiC/DLC/SiC/DLC was prepared. The multi-layered structure was designed to reduce the possibility of pinholes that may grow throughout the entire film. The thick outermost layer of DLC was to maintain a hard layer to protect the surface from mechanical damage. DLC coating is harder than the SiC coating. Table 2 summarizes all the PIID DLC coatings prepared for this investigation.

After the deposition, scanning electron microscopy (SEM) with energy dispersive spectroscopy was used to examine the multi-layer coating structure, while Raman spectra were acquired using a Renishaw Raman imaging microscope that operated at 785 nm. Wavenumber calibration was carried out using the 520.5 cm^{-1} line of a silicon wafer. Spectra were recorded by scanning the 150 to 3000 cm^{-1} region for a total acquisition time of 5 min.

TABLE 2

Deposition parameters and properties of the PIID DLC coatings

Coating Type	Deposition Parameters											Properties					
	V_{Peak} [V]	I_{Peak} [A]	F_{Puls} [Hz]	L_{Puls} [µs]	P [mTorr]	t_{Dep} [min]	Ar flow [sccm]	TMS flow [sccm]	C_2H_2 flow [sccm]	HMDSO flow [g/hr]	HFPO flow [sccm]	Thickness [µm]	Hardness [GPa]	Young's modulus [GPa]	COF	Wear rate [mm^3/N.m]	Ra (AFM) [nm]
Standard DLC	1.38	43	1000	20	10	120	0	0	80	0	0	10.05	4.3	24.7	0.30	1.4×10^{-6}	18.4
Multi-layer Si-DLC	1.36	50–55	1000	20	10	120	0	20	80	0	0	7.5	6.8	16.4	0.20	9.8×10^{-6}	14.5
Si-F-O-DLC	1.1	40	3050	20	20	180	5	0	0	6	150	7.2	1.3	6	0.62	4.7×10^{-6}	10.2
Thick DLC	1.6	102	2050	20	10	270	0	0	127	0	0	21	6.3	152	0.32	3.4×10^{-6}	35.9

Mortar Specimens

A total of 25 mortar specimens were prepared and tested in this investigation. The mortars contained different amounts of admixed chlorides. Chloride ions were introduced as part of the mixing water, using reagent grade NaCl (99.4% purity) to attain the desired chloride content. The mortar mix groups were generally prepared following the ASTM C-305-94 Standard Test Method (*18*). The fine aggregate used for the mortar mix groups was Ottawa sand that had an absorption capacity of 0.2% and water content of 0.9%.

The mortars were cast in cylindrical plastic molds of 4 in. (10.2 cm) diameter by 4.5 in. (11.5 cm) long. The total chloride content ranged from 0 to 5% wt. of mortar. The cement content was 30.5–31.7 lb/ft^3 (489–508 kg/m^3) of mortar and the water-to-cement (w/c) ratio was 0.50. Two mortar cylinders were prepared for each chloride concentration and coating type. The sand-to-cement ratio used for all mortar series was set to 2.75. The mix proportions of the mortar batches are given in Table 3.

Each mortar cylinder had a single coated rebar positioned at the center of the cylinder. The nominal area, A, of the coated rebar in contact with the mortar was 26.5 cm^2 (4.1 in.^{2}). The coated rebars were #3 (nominal 0.37 in. (0.95 cm) diameter) and 6 in. (15.2 cm) long. Prior to coating application, the rebars were sandblasted to remove any existing iron oxide followed by rinsing in acetone. Figure 9 shows a picture and schematic of the mortar specimens. The area of the rebar protruding outside the mortar was coated with microstop to prevent corrosion at the interface.

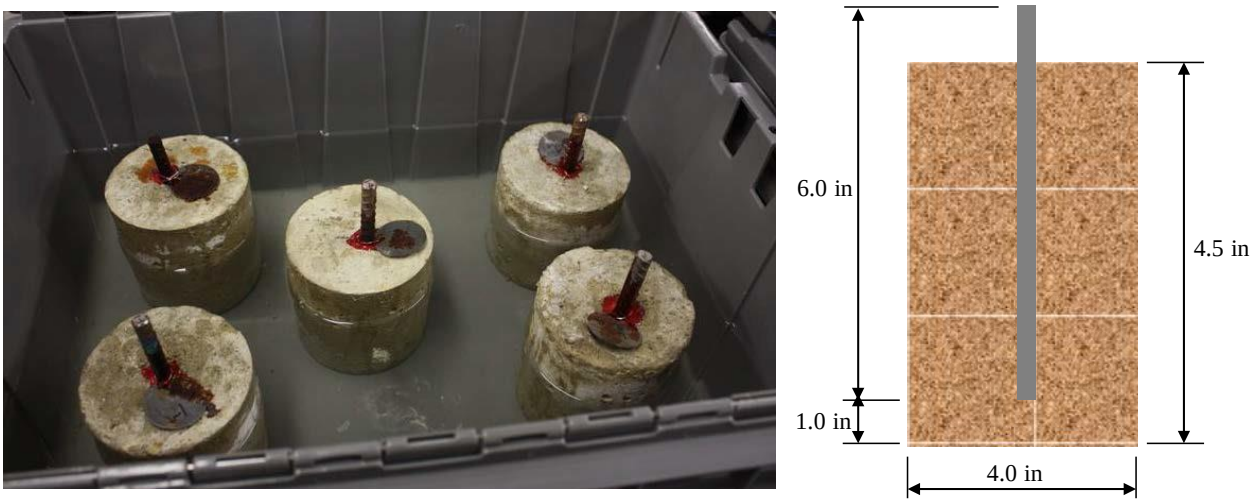

FIGURE 9 Picture and schematic of the mortar specimens.

TABLE 3
Mortar specimen mix proportions

Batch Number	Cement lb/ft^3 (kg/m^3) mortar	Water lb/ft^3 (kg/m^3) mortar	Sand lb/ft^3 (kg/m^3) mortar	Chloride (% wt. mortar)
1	31.7 (508)	15.8 (254)	87.3 (1,398)	0
2	31.5 (504)	15.7 (252)	86.5 (1,386)	0.5
3	31.3 (502)	15.6 (251)	86.0 (1,379)	1.0
4	30.9 (496)	15.5 (248)	85.1 (1,363)	3.0
5	30.5 (489)	15.2 (244)	83.9 (1,344)	5.0

The mortar cylinders were demolded 24 hours after casting and cured inside a ~100% relative humidity chamber for 30 days, occasionally lightly mist spraying the mortar surface with distilled water to keep the surface slightly wetted. Afterwards, the specimens were partially immersed in simulated seawater for up to 140 days at 77°F (25°C).

The potential of the rebar in each mortar specimen was periodically measured with respect to an external saturated calomel electrode (SCE) in contact with the surrounding solution[1]. Coating performance was examined by linear polarization resistance (LPR) and EIS measurements. For both electrochemical techniques, the rebar was connected

as a working electrode to a potentiostat. The reference electrode was a SCE partially immersed in the solution surrounding the mortar specimens. The counter electrode was a stainless steel mesh placed around the outer diameter of the mortar specimens. For the LPR measurements, the impressed potential was varied from the corrosion potential in the cathodic direction, by the amount of 10 mV. The Stern-Geary relationship was used to compute the corrosion rate:

$$i = B/R_P A$$

where B was estimated to be 0.026 V (*19*) and R_P is the nominal polarization resistance obtained by LPR in ohms.

The EIS measurements were conducted at the open circuit potential in the frequency range from 100 kHz to 10 mHz using a sinusoidal signal of 20 mV_{RMS} amplitude. Data were collected in this frequency range at 5 points per decade of frequency.

At the end of exposure, the mortar specimens were removed from the solution, sectioned, and the coated rebar was inspected for coating breaks and corrosion.

EXPERIMENTAL RESULTS

Characterization and Optimization of the S-DLC Coating

Initially in this investigation, SEM analysis revealed an unanticipated problem of cracking in the s-DLC films deposited on the rebar surface. These cracks were on the micro-scale and were evident in SEM analysis (Figure 10). SwRI investigated methods to mitigate this cracking, including altering the parameters in the pyrolysis step varying heating and cooling rates and exploring alternative wet-coating techniques. Multiple layers of s-DLC films were also applied to the rebars in efforts to mitigate cracking. Both approaches were successful in mitigating the formation of cracks.

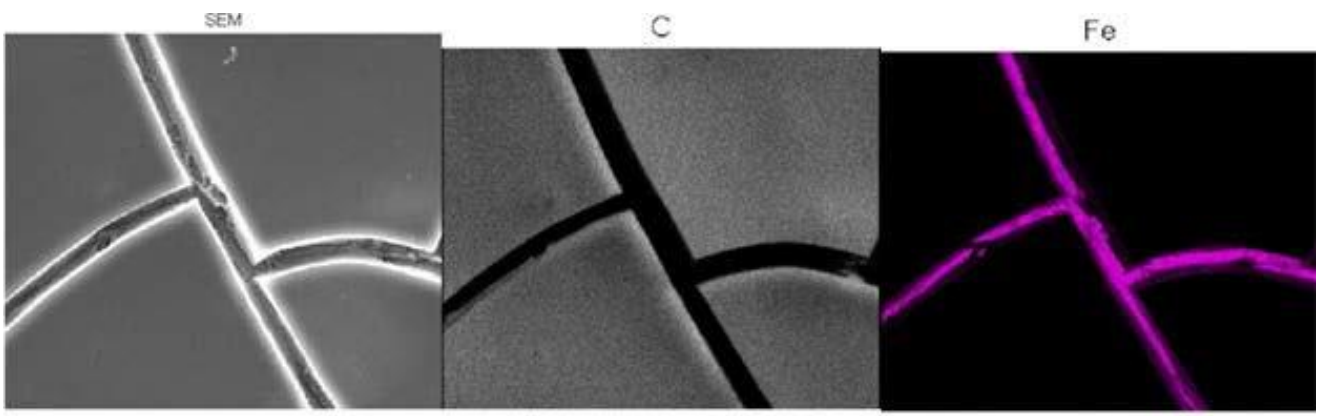

FIGURE 10 SEM images and corresponding elemental carbon and iron Energy-Dispersive Spectroscopy (EDS) maps revealing micro-cracking in s-DLC coating on rebar substrates.

The synthetic procedure developed by SwRI to produce the s-DLC proved to be consistent in yielding product with reproducible chemical properties as determined by FTIR spectroscopy, absorption spectroscopy, and thermogravimetric analysis (TGA). Correlation of FTIR and absorption spectral data suggested that a phenylcarbyne-type unit containing nitrogen is the primary structural feature with other impurities (C=C and C-O-C) present (Figure 11). The FTIR spectra are similar to those previously reported for poly(phenylcarbyne) molecules (*8*). The dominant features in the FTIR spectra are a strong band at 1068 cm^{-1} which arises from C-C stretching and bands at 2975 and 2870 cm^{-1} characteristic of aliphatic (sp^3) C-H stretching. The bands at 2930 cm^{-1} and 1642 cm^{-1} can be attributed to impurities of incorporated tetrahydrofuran (THF), and C=C conjugated polyacetylene molecules and low molecular weight oligomer side products. A band at 3500 cm^{-1} arises from adsorbed water.

Weak bands present correspond to mono-substituted phenyl groups and C-N vibrations. The absorption spectra exhibited an intense broad absorption that starts at a wavelength of 250 nm and decreases into the visible to 450 nm. This feature of the absorption spectra is analogous to those reported for polyphenylcarbyne molecules and to those produced by electronic transfer by way of rigid non-conjugated C-C bonds (*8*, *20*).

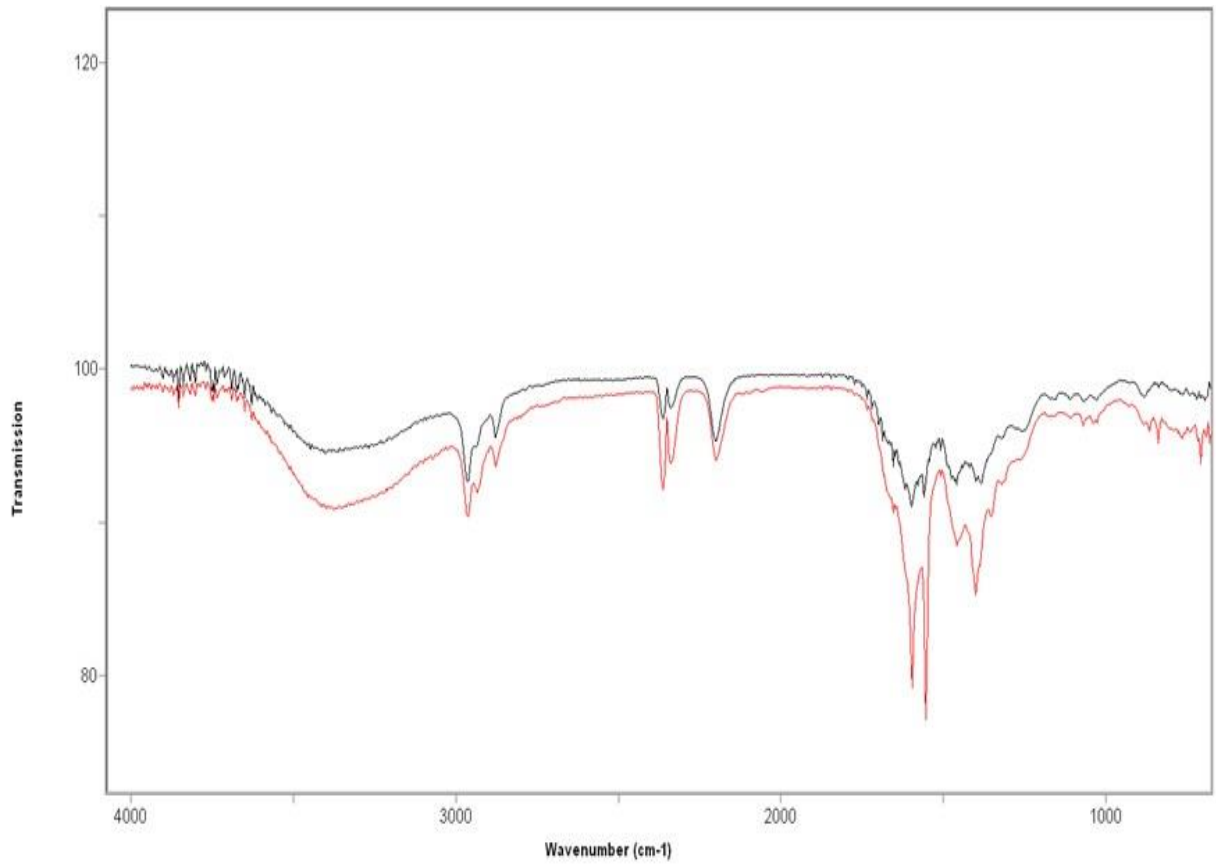

FIGURE 11 FTIR spectra of raw polymer precursor product from two separate syntheses illustrating reproducibility of method. Spectra further indicate a phenylcarbyne-type unit as primary structural feature with other impurities present.

Figure 12 shows typical TGA and DTA curves of purified polymer powders. DTA and TGA show that thermal decomposition begins at 200°C and is complete at 842°F (450°C) with a second decomposition beginning at 1472°F (800°C) to 1832°F (1000°C), having reached a final weight of ~36% of the initial. Endothermic reactions occurring at temperatures lower than 200°C are associated with volatilization of water, incorporated THF, and other transients. The conversion of the polymer precursor to s-DLC was investigated as a function of temperature. Polymer precursor powders were heated at 392°F, 1112°F, and 1832°F (200°C, 600°C, and 1000°C) for 2 hours in a vacuum. The resulting heated powders were investigated with Raman spectroscopy and quantitative elemental analysis by ICP-MS (Analytical MicroLab, Inc.).

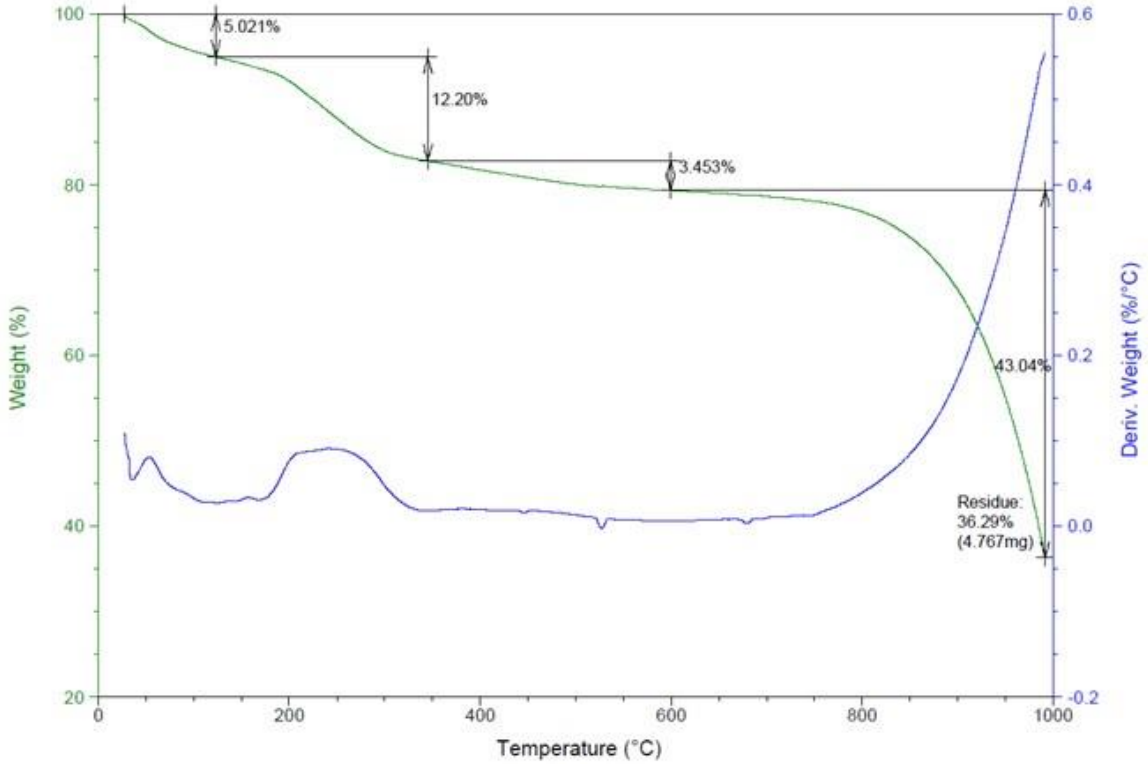

FIGURE 12 Thermal analysis by TGA and DTA of purified polymer powder.

Raman spectroscopy provides information on the bonding structure of DLC. Raman spectrum of DLC and most disordered carbons are dominated by the G and D modes of graphite. The G mode is the stretching of any sp^2 sites, either C=C chains or in aromatic rings. The D mode is the breathing mode of those sp^2 sites in aromatic rings (not in C=C chains). Raman characteristics of the polymer showed a slight dependence on the temperature of heat-treatment. Raman spectra of all the heated polymer precursors exhibit broad Raman feature between 1200 cm^{-1} and 1600 cm^{-1}, characteristic of DLC and amorphous carbon coatings. The Raman spectra of the 392°F (200°C) product corroborate the TGA/DTA data and indicate decomposition of polymer precursor has initiated (Figure 13a). The resulting product is brownish-black powder that is partly soluble in organic solvents. The broad peak at 1330 cm^{-1} related to sp^3 C phase slightly sharpens and increases with heat treatment to 600°C (Figure 13b) and then again to 1832°F (1000°C) (Figure 13c). The resulting products of these higher heat treatments are grayish-black abrasive powders. These results further support conversion to s-DLC and increasing sp^3 C content with increasing temperature.

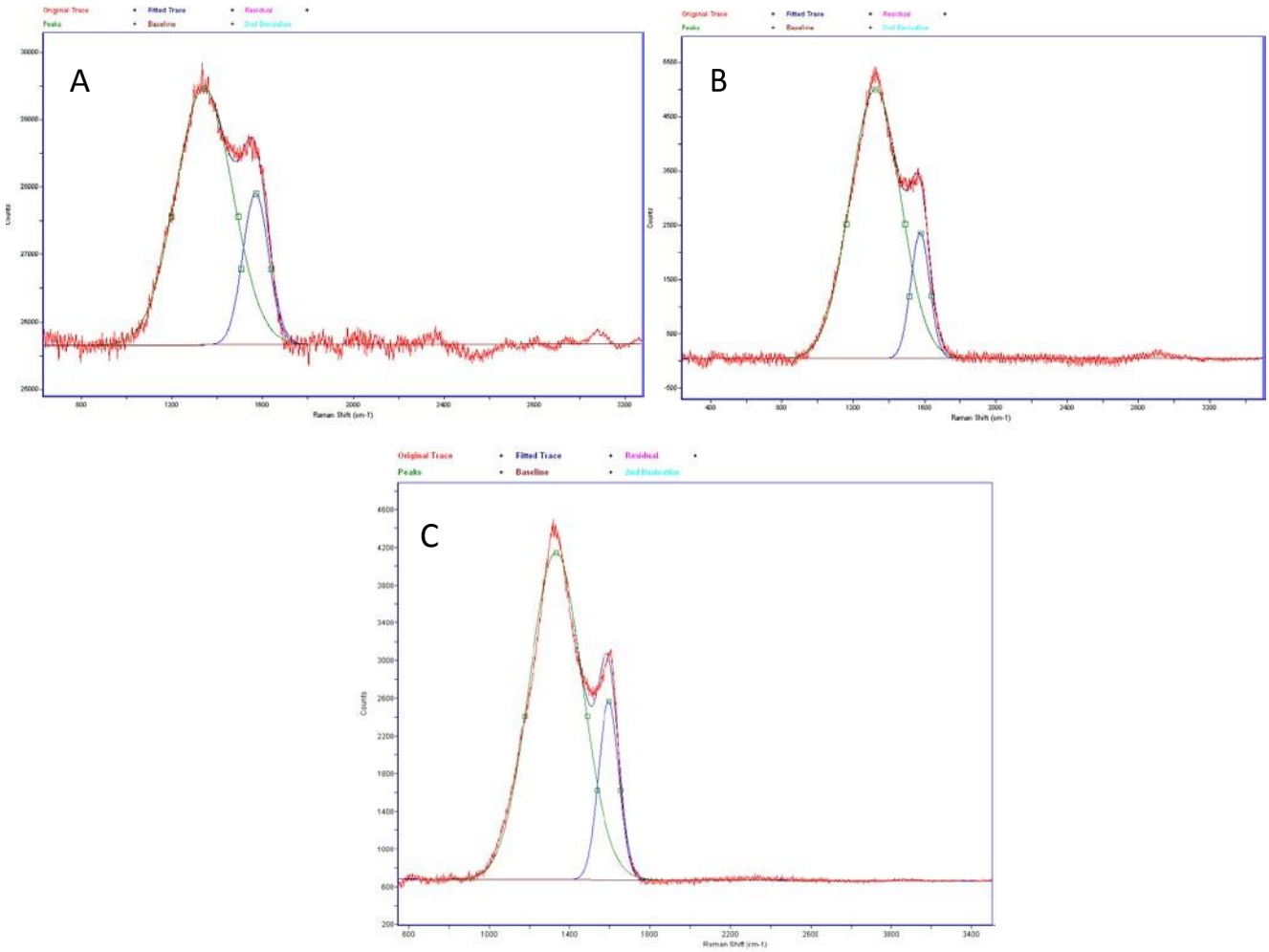

FIGURE 13 Raman spectra of polymer precursor as a function of temperature at (a) 392°F (200°C), (b) 1112°F (600°C), and (c) 1832°F (1000°C).

A typical cross-section SEM image and the corresponding Raman spectrum of an s-DLC film are shown in Figure 14. Figure 14 also shows the nanoindentation analysis on s-DLC film (CSM Instruments). The average measured hardness for three indentations was 12.1 ± 1.1 GPa. Water contact angle measurements on DLC films are commonly used to access the surface energy of the film. DLCs are considered hydrophobic, having contact angles with water ranging from 55° to 80° (*21*). The water contact angles for s-DLC are within this range with an average of 57.5° ± 3.2° (Figure 15). Altogether, these results have begun the foundation for scaling this new process into pilot process for depositing and evaluating s-DLC on components with large dimensions.

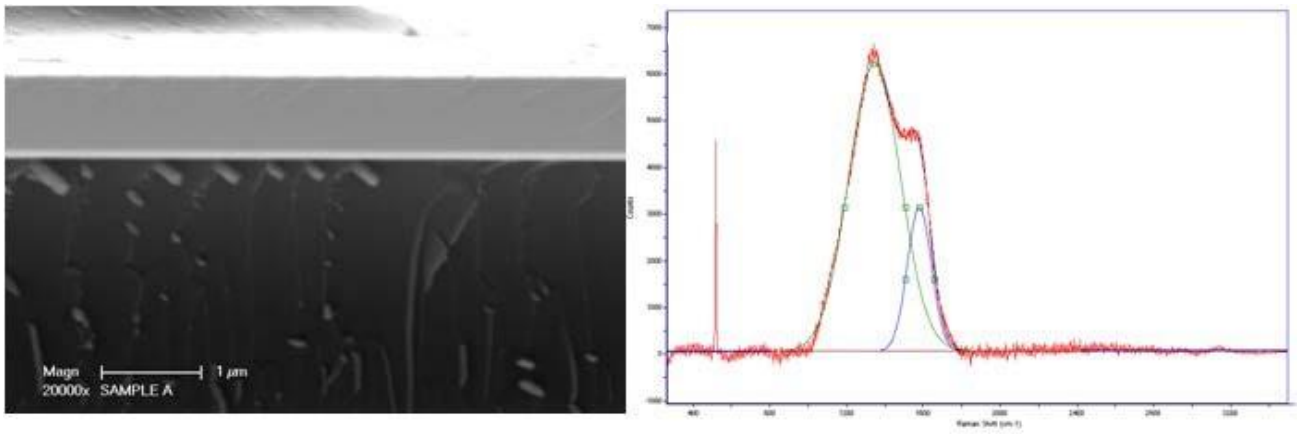

FIGURE 14 Representative (a) cross-section SEM image, and (b) Raman spectrum of thin s-DLC coating (spray-coated and heated to 600°C for 2 hours in vacuum).

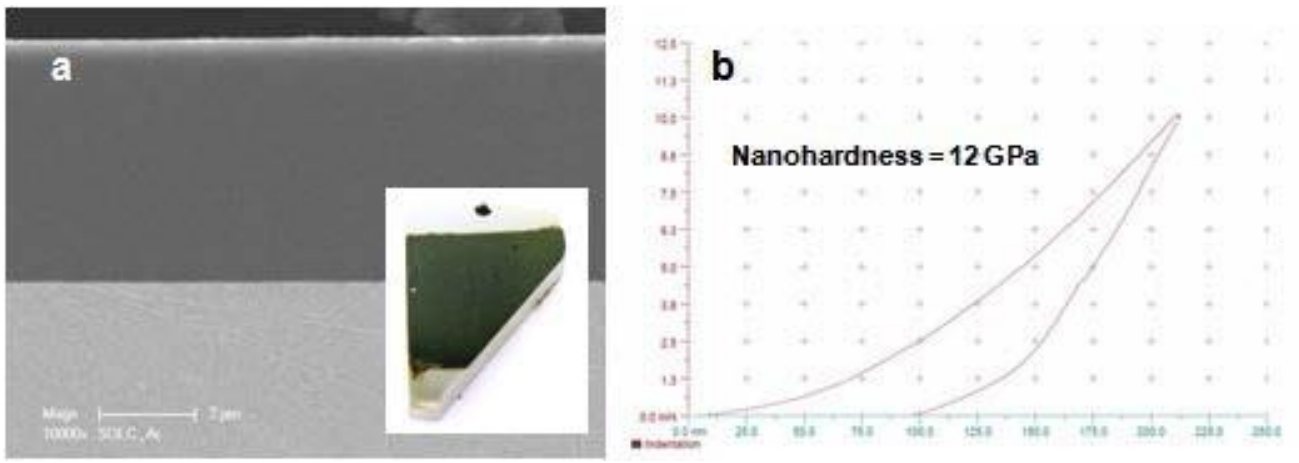

FIGURE 15 (a) Cross-section SEM images and photograph (inset) of machined edges of s-DLC-coated steel substrate. (b) Representative force displacement curve for nanoindentation on s-DLC film. Average hardness measured for three indentations was 12.1 ± 1.1 GPa.

FIGURE 16 Representative water contact angle analysis on s-DLC coating. The water contact angles for s-DLC averaged 57.5° ± 3.2°.

The optimized s-DLC coatings exposed to simulated pore solution (pH = 13.3) without chlorides for up to 45 days had an average open circuit potential of −0.3 V vs. SCE. This potential value is in agreement with the large impedance results recorded during the exposure (Figure 17), in agreement with the absence of coating degradation and corrosion of the underlying substrate. When the chloride concentration was increased in the range from 0 to 1.5 mol/L (Figure 18), the low frequency end of the impedance spectra showed a decrease in the impedance modulus (about one order of magnitude), indicative of an onset of coating degradation and subsequent corrosion of the substrate. For comparison, a vacuum-deposited DLC coating was also tested on companion coupons. The companion vacuum-deposited DLC showed an impedance modulus about one order of magnitude larger (2×10^5 ohm) than that of the s-DLC coating for the same chloride concentration. These results are consistent with the impedance results reported (*22*). This demonstrated that the s-DLC coating has a lesser protective capability than the traditional DLC coating. Figure 19 shows images of the s-DLC and traditional vacuum-1.6 deposited DLC coatings after being exposed to concrete pore solution (pH = 13.3), with chloride concentration

ranging from 0 to 1.5 mol/L. The coating surface showed discoloration more notable for the s-DLC coating than the traditional vacuum-deposited DLC coating.

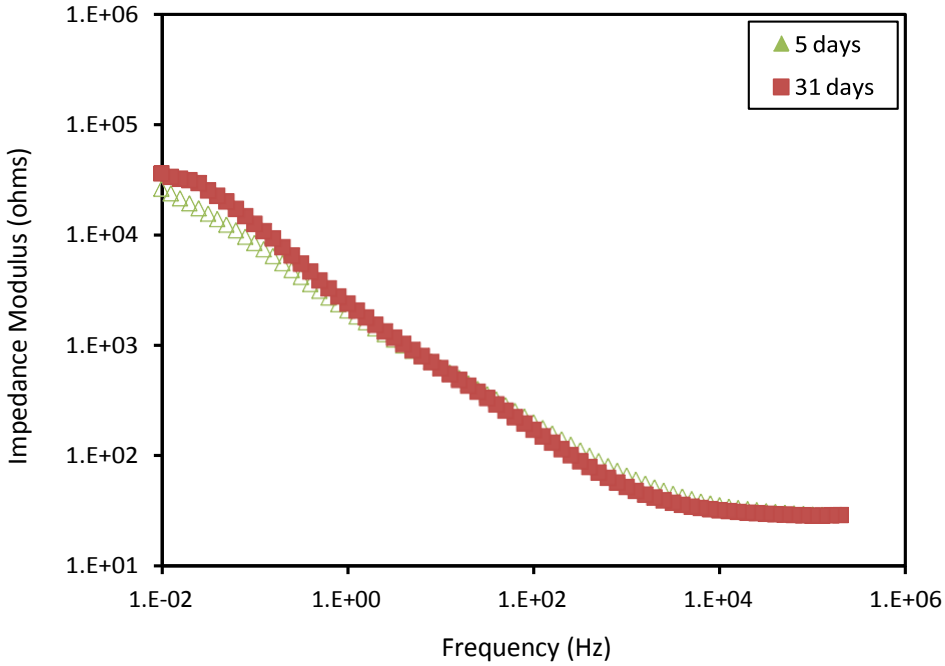

FIGURE 17 Impedance values of flat s-DLC-coated coupons exposed to simulated concrete pore solution (pH = 13.3) without chlorides.

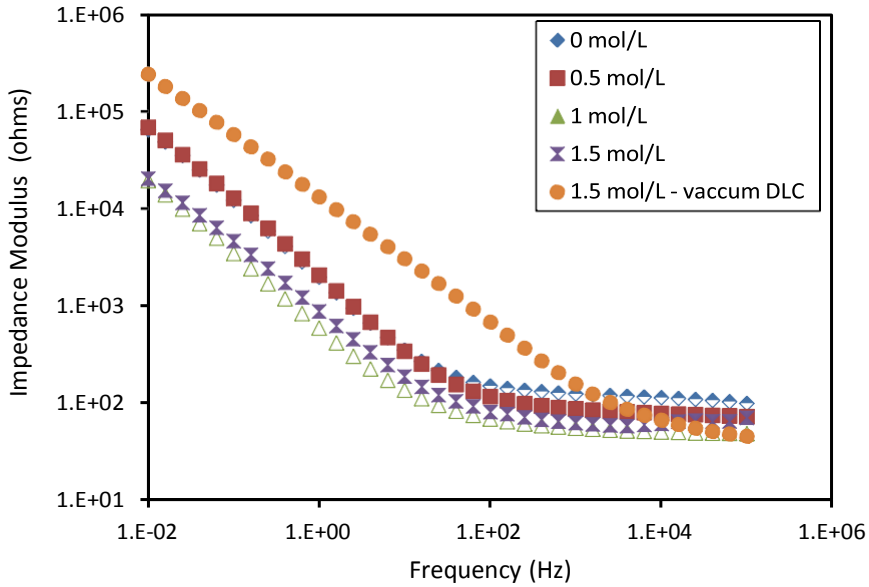

FIGURE 18 Impedance values of flat s-DLC-coated coupons exposed to simulated concrete pore solution (pH = 13.3) with chloride concentrations ranging from 0 to 1.5 mol/L. Vacuum-deposited DLC coating was also plotted for comparison.

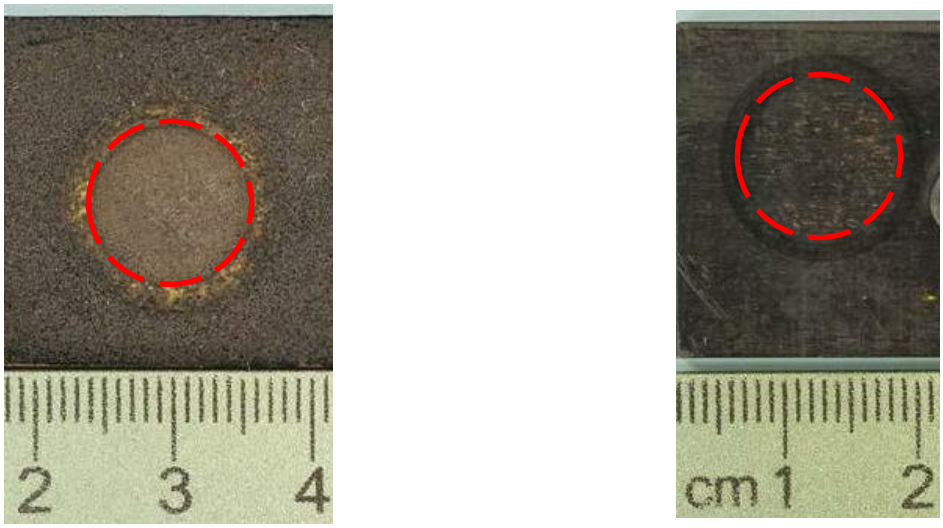

(A) (B)

FIGURE 19 Surface appearance of the s-DLC (A) and traditional vacuum-deposited DLC (B) coatings after exposure to simulated concrete pore solution (pH = 13.3) with chloride concentration ranging from 0 to 1.5 mol/L. Dotted circles denote the area of sample exposed to solution

Characterization of the PIID DLC Coatings

Two-dimensional surface morphologies of the PIID DLC coatings deposited on the rebar using the PIID process were measured using an atomic force microscope (AFM). The roughness (Ra) values of the coatings are summarized in Table 2. The coatings were, in general, smooth and the roughness was in the order of tens of nm. The vacuum-deposited standard DLC and multi-layer Si DLC coatings exhibited similar surface morphology in which carbon clusters were uniformly distributed on the surface (Figures 20 and 21). Coatings show Ra values of 18.4 nm and 14.5 nm, respectively. The Si-F-O DLC coating is observed to be smoother than the first two coatings (Figure 22), with the Ra dropping to 10.2 nm. The carbon clusters get coalesced and become denser in the thick DLC coating, which also showed the largest Ra of 35.9 nm due to the larger thickness of the coating (Figure 23). The denser surface morphology of the thick DLC coating is mainly related to the high peak current applied during the coating deposition.

The cross-sectional microstructure of the PIID DLC coatings deposited on the rebar was studied using scanning electron microscopy (SEM). As shown in Figures 20–23, all coatings showed good bonding with the rebar surface and a successful coverage of the rough surface of the rebar. The PIID DLC coatings also exhibited dense microstructure without observation of voids and macro-particles. As shown in Figure 20, the standard DLC coating showed a columnar grain structure. The multi-layer Si DLC coating showed a multi-layer structure in which the Si rich and C rich (dark) DLC monolayers were grown alternatively throughout the coating thickness (Figure 21). The Si-F-O DLC coating (Figure 22) exhibited a dense amorphous-like structure that contains two layers; the bottom layer is a Si doped carbon layer while the top light layer is a carbon layer with the incorporation of hexafluoropropylene oxide (HFPO), which was found to have a positive effect on improving the hydrophobic property of the DLC coatings on the surface. Figure 23 shows the microstructure of the thick DLC coating. The thick DLC coating exhibited further improved density with the disappearance of columnar grains. This result is consistent with the observation from the AFM study.

As summarized in Table 2, the multi-layer Si DLC, standard DLC, and thick DLC coatings exhibited high hardness values of 6.8 and 6.3 GPa, respectively. The Si-F-O DLC coating with the incorporation of HFPO on the surface showed a low hardness of 1.3 GPa. Dry sliding wear tests of these coatings against an Al_2O_3 ball in the ambient air showed that only the Si-F-O DLC coating showed a high COF of 0.62, while other three DLC coatings exhibited relatively low COF in the range of 0.20 to 0.32.

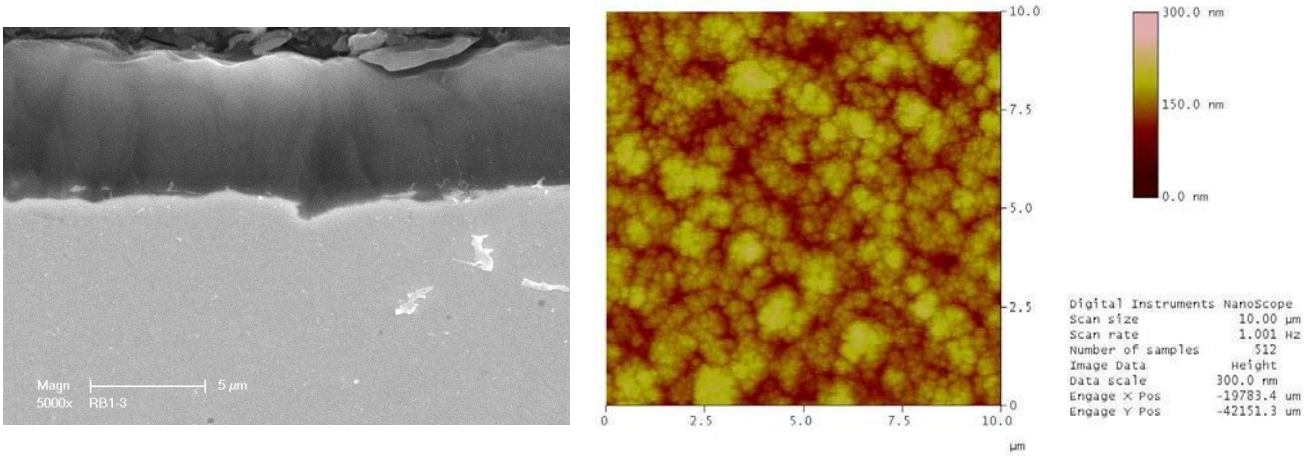

FIGURE 20 SEM and two-dimensional AFM analyses of the standard DLC coating.

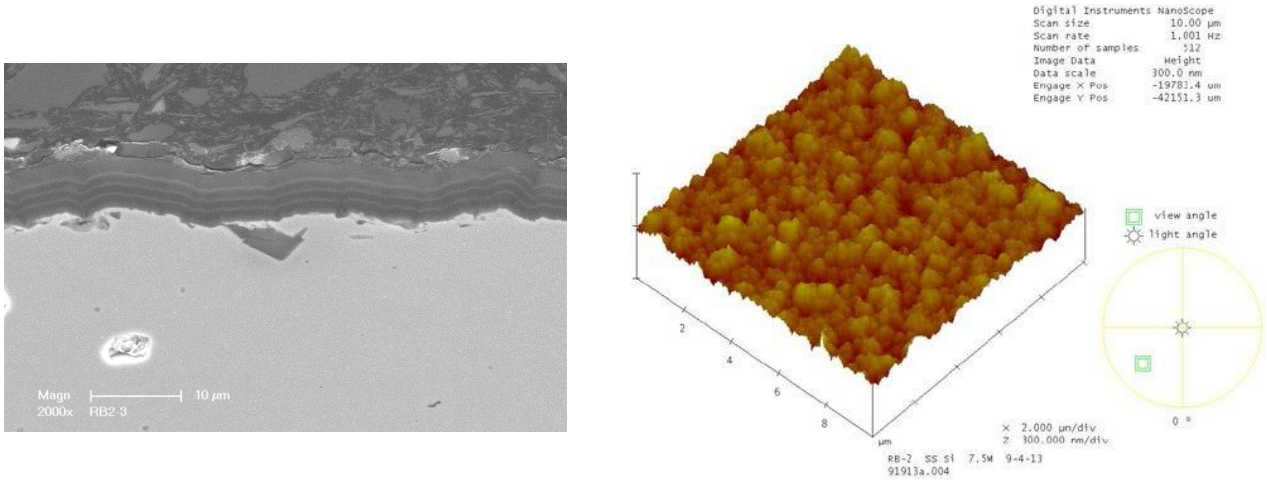

FIGURE 21 SEM and two-dimensional AFM analyses of the multi-layer Si DLC coating.

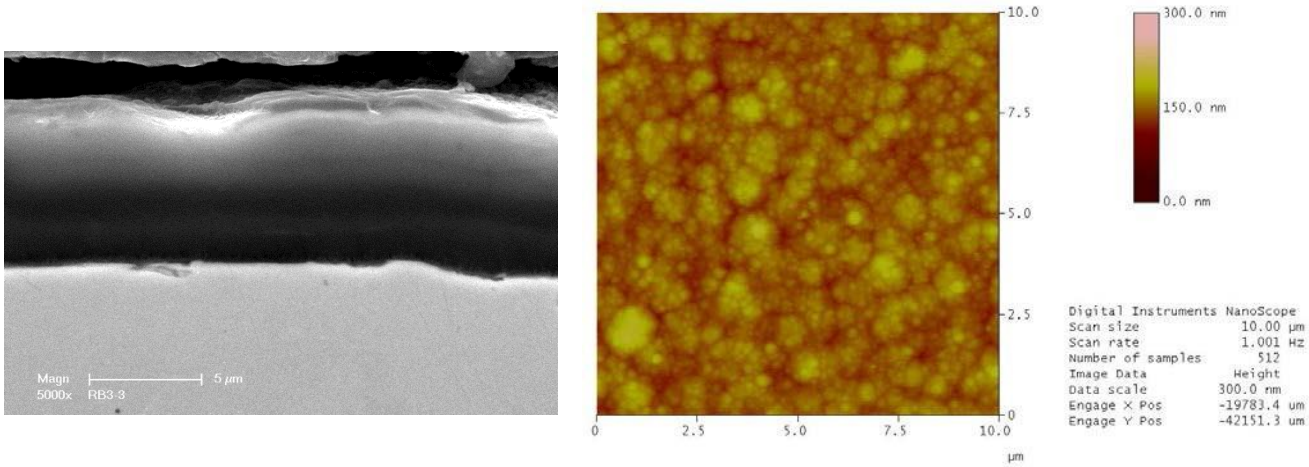

FIGURE 22 SEM and two-dimensional AFM analyses of the Si-F-O DLC coating.

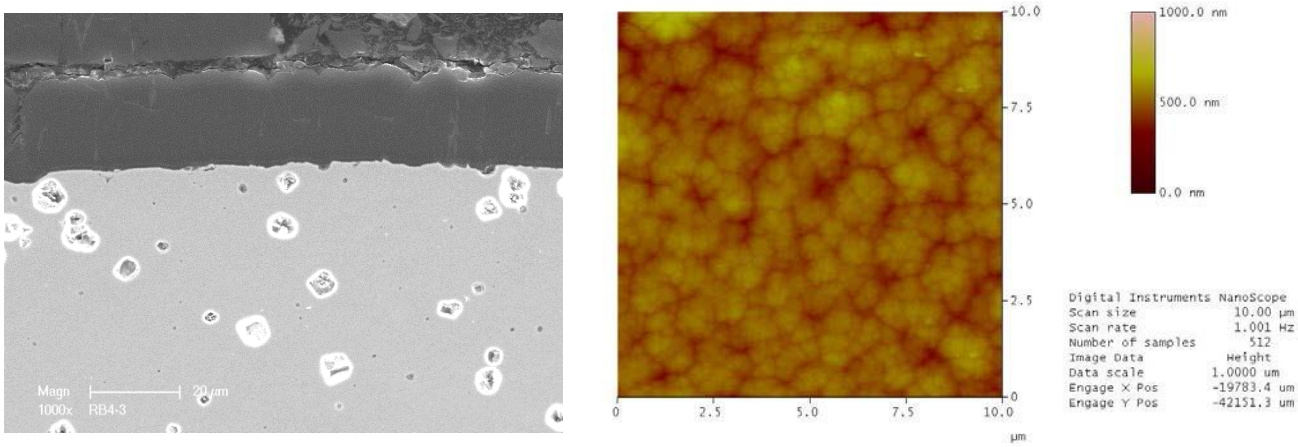

FIGURE 23 SEM and two-dimensional AFM analyses of the thick DLC coating.

Coating Performance in Mortars

Figures 24–28 show the results of the linear polarization resistance, converted to mils per year (mpy), for the coated rebars embedded in mortars admixed with various chloride concentrations. Note that the results are not to be interpreted quantitatively. In coated specimens, corrosion is likely not uniform. Rather, it is concentrated at localized defective areas (such as pinholes, voids, etc.). Given that DLC coatings are electrical insulators, polarization only occurs at these defective areas, which cannot be accounted for in the calculation of the polarization resistance term. The linear polarization resistance results may indicate the presence of corrosion in the defective areas, but an evaluation of the extent of corrosion must rely on the visual inspections and microscopic investigations.

Some guidelines have been developed to establish a relationship between corrosion current density and corrosion rate, as shown in Table 4.

TABLE 4
Relationship between corrosion current density and corrosion rate

Corrosion Current Density, µA/cm^2	Corrosion Rate
<0.1	Negligible
0.1–0.5	Low
0.5–1.0	Moderate
>1.0	High

Under these assumptions, the linear polarization results showed that for the case of 0% chloride content, corrosion rates were negligible/low (<0.1 mpy) for the s-DLC, Si-F-O DLC, and thick DLC coatings. For the standard DLC and multi-layer Si DLC coatings, corrosion rates were moderate (0.65–0.90 mpy). As expected, as the chloride concentration increased, corrosion rates also increased (Figure 29). This increase in corrosion rates was more notable for the s-DLC coating than the other coatings. By the end of the 140-day exposure period, the corrosion rate for the s-DLC coating in 0.5% chloride concentration was high (1.9 mpy), moderate (0.55 mpy) for the standard DLC and multi-layer Si DLC coatings, and negligible (<0.07 mpy) for the Si-F-O DLC and thick DLC coatings. This indicates that coating defects are likely to be present in the s-DLC, standard DLC, and multi-layer Si DLC coatings. Similar trends were recorded for the 1% and 3% chloride contents. For the 5% chloride concentration, all of the DLC coatings, except for the thick DLC coating, showed high corrosion rates (>1.4 mpy), whereas the thick DLC coating displayed a moderate corrosion rate (0.75 mpy).

The EIS results of the DLC coatings obtained after 86 days of exposure are shown in Figures 30–34. The results show comparable trends as those recorded by the linear polarization measurements. Overall, the low frequency impedance moduli decreased with an increase in chloride concentration. The decrease in the impedance modulus was more notable for the s-DLC coating than the other coatings. As reported by others (*23*, *24*), polarization

resistance values of epoxy-coated rebars in chloride-contaminated concretes can be as low as 20 kohm. This value is about one order of magnitude larger than the polarization results of the DLC coatings obtained in this investigation.

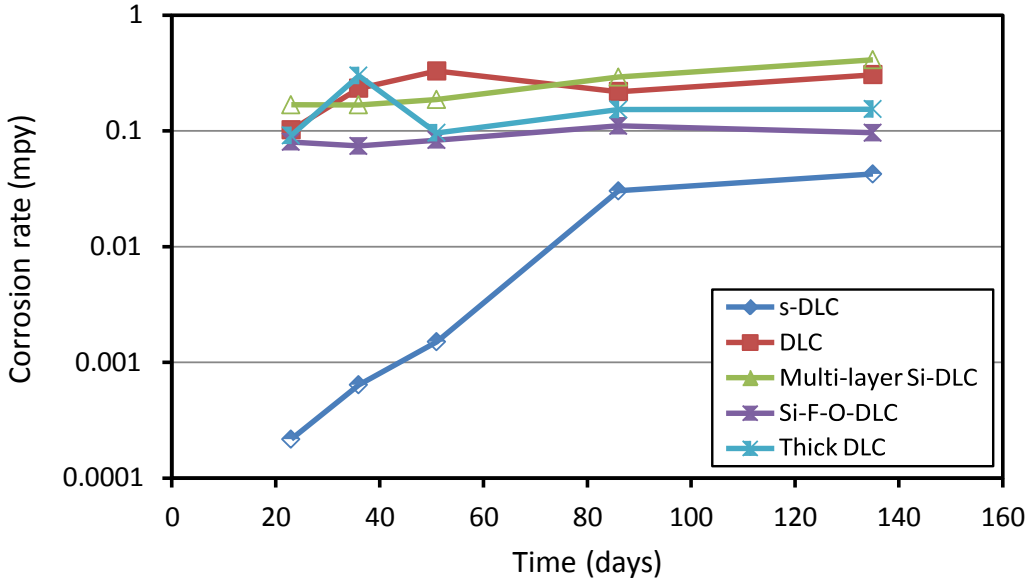

FIGURE 24 Linear polarization resistance results of the DLC coatings embedded in mortars admixed without chlorides (batch 1).

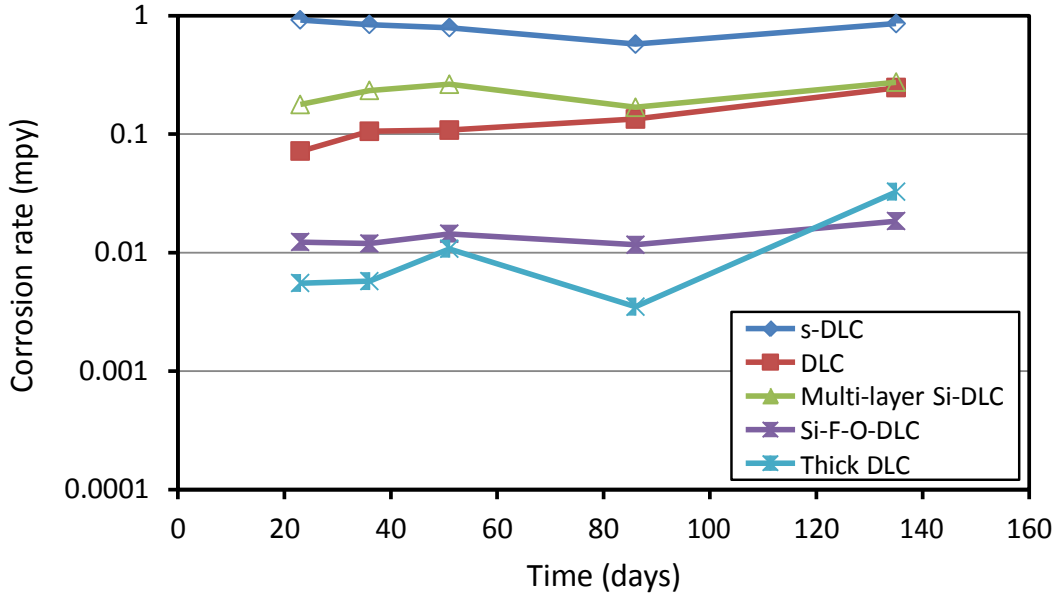

FIGURE 25 Linear polarization resistance results of the DLC coatings embedded in mortars containing 0.5% chloride by wt. of mortar (batch 2).

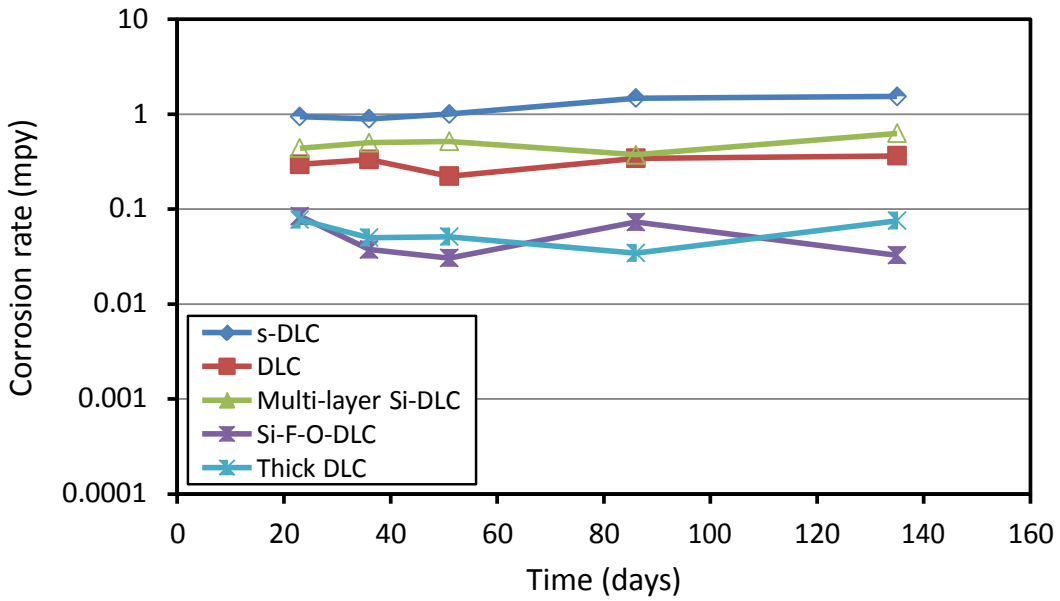

FIGURE 26 Linear polarization resistance results of the DLC coatings embedded in mortars containing 1% chloride by wt. of mortar (batch 3).

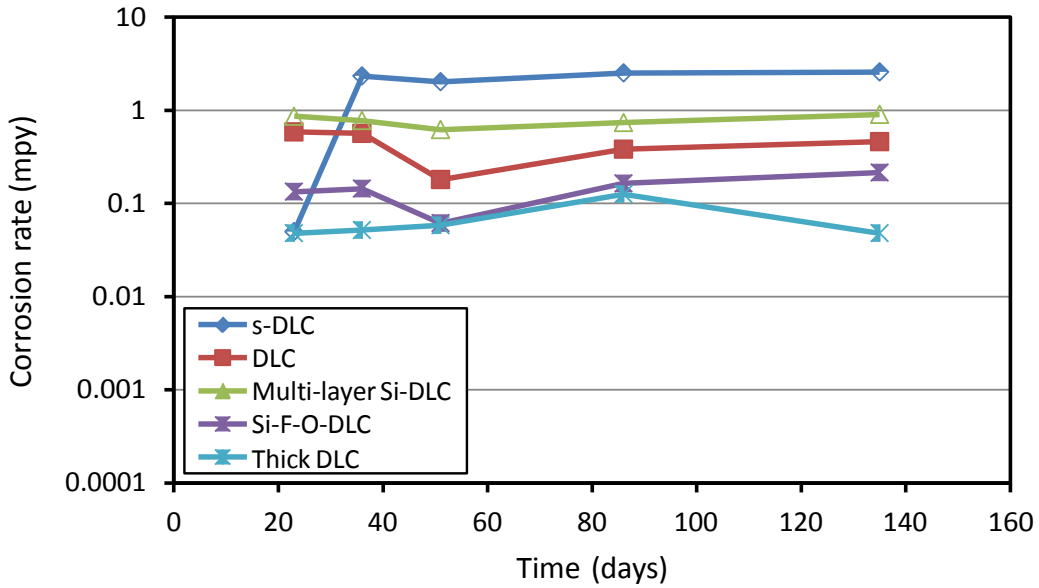

FIGURE 27 Linear polarization resistance results of the DLC coatings embedded in mortars containing 3% chloride by wt. of mortar (batch 4).

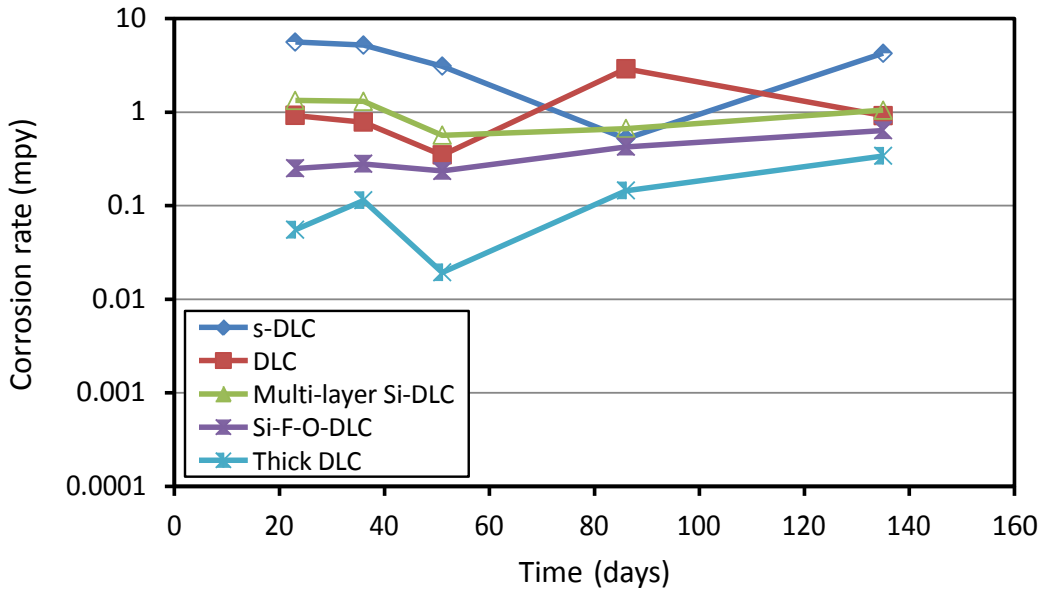

FIGURE 28 Linear polarization resistance results of the DLC coatings embedded in mortars containing 5% chloride by wt. of mortar (batch 5).

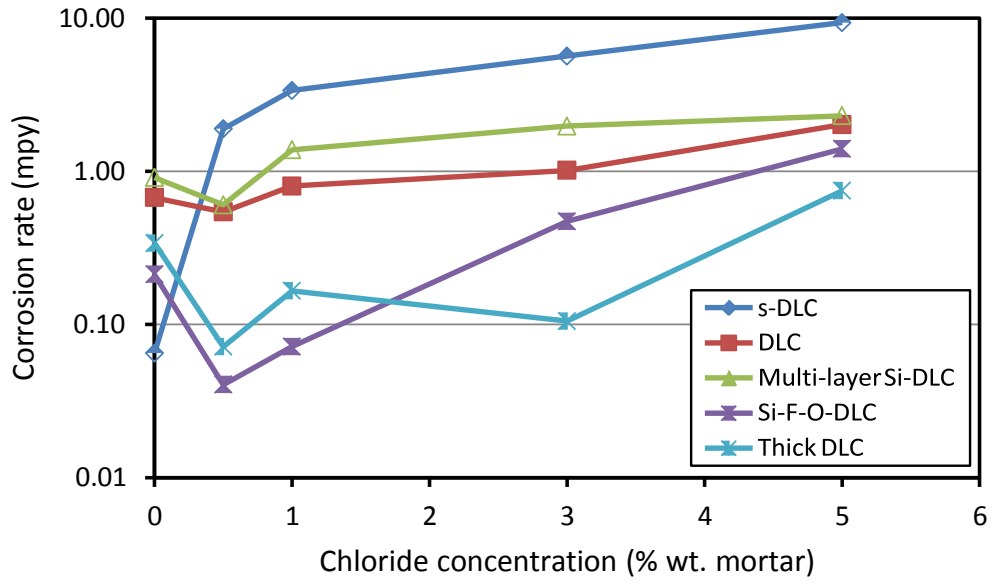

FIGURE 29 Linear polarization resistance results as a function of chloride concentration of the DLC coatings embedded in mortars obtained by the end of the 140-day exposure.

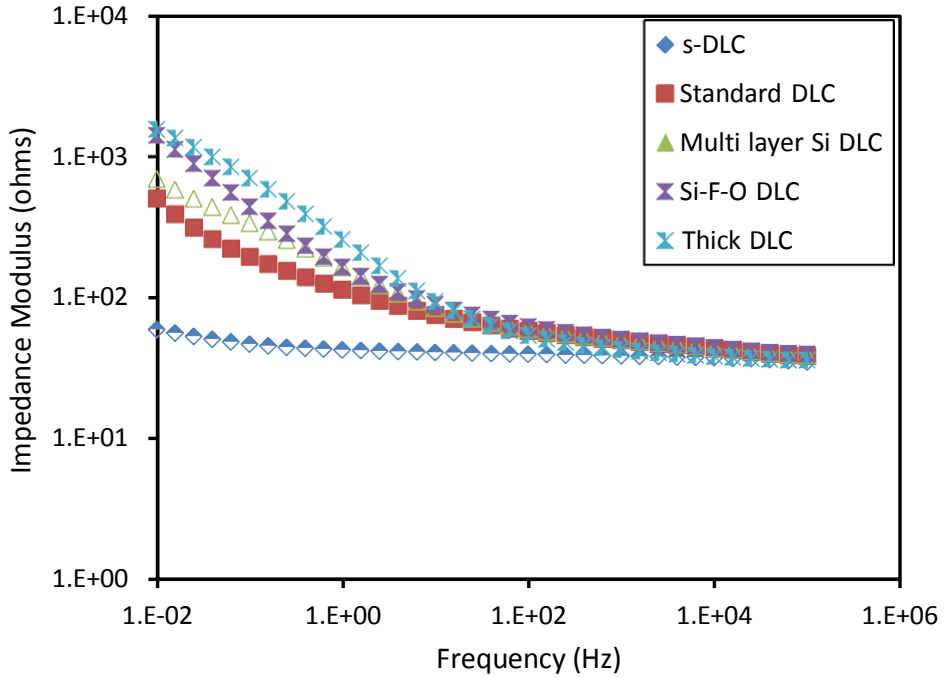

FIGURE 30 Impedance values of the DLC coatings embedded in mortars admixed without chlorides (batch 1) obtained after 86 days of exposure.

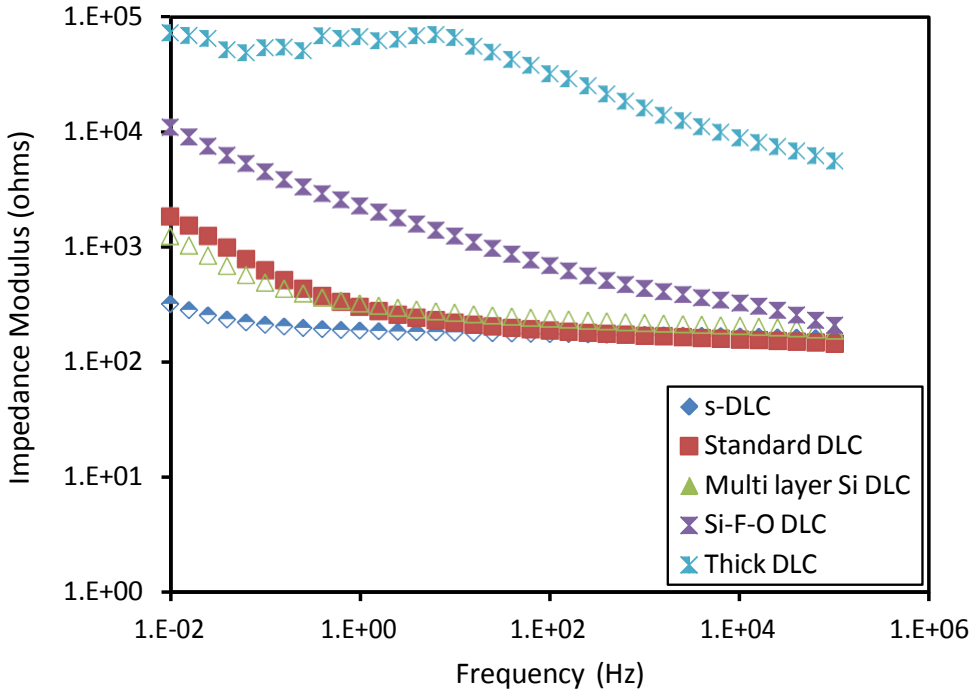

FIGURE 31 Impedance values of the DLC coatings embedded in mortars containing 0.5% chloride by wt. of mortar (batch 2) obtained after 86 days of exposure.

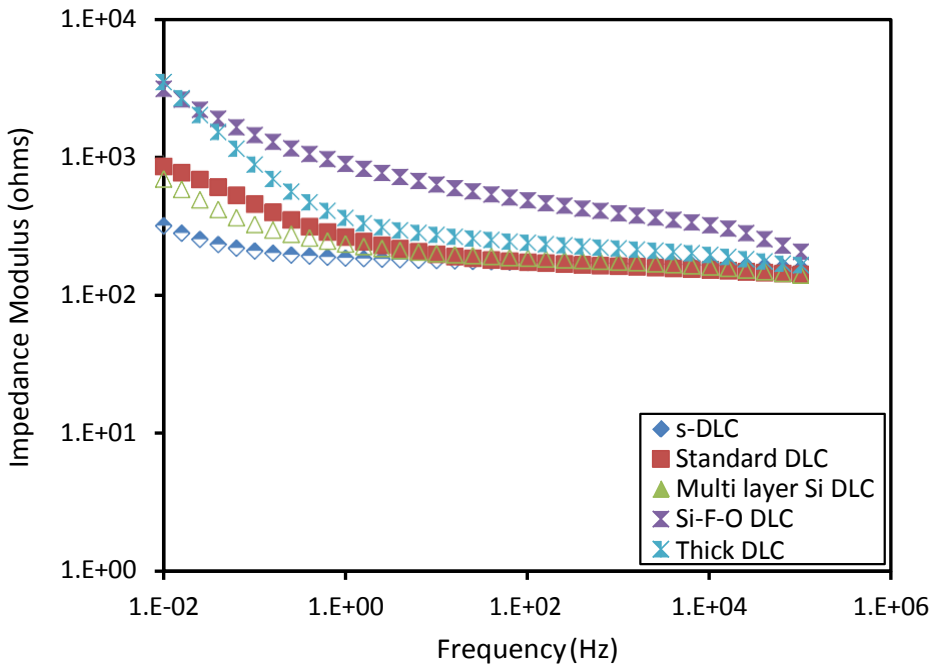

FIGURE 32 Impedance values of the DLC coatings embedded in mortars containing 1% chloride by wt. of mortar (batch 3) obtained after 86 days of exposure.

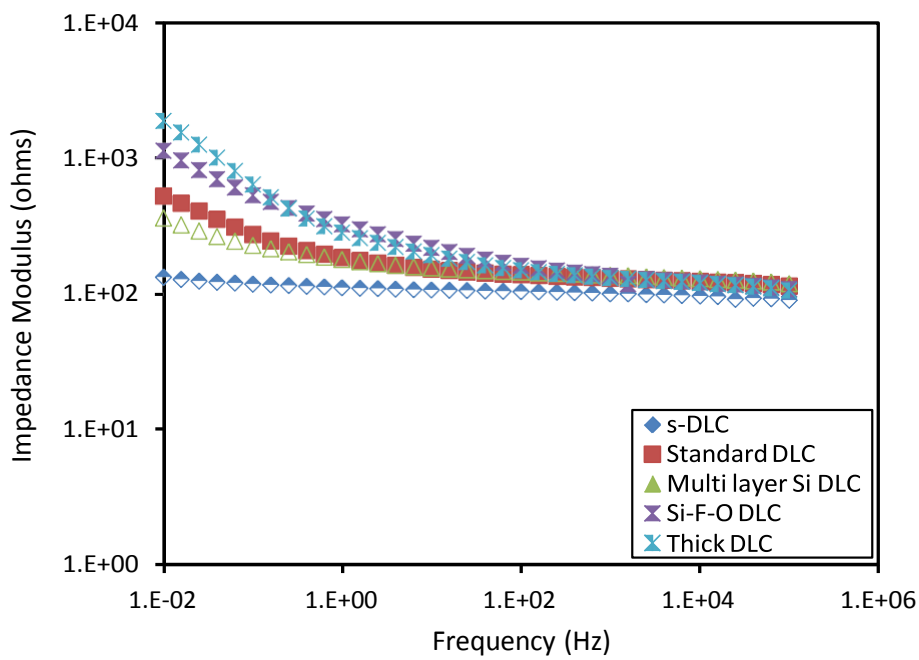

FIGURE 33 Impedance values of the DLC coatings embedded in mortars containing 3% chloride by wt. of mortar (batch 4) obtained after 86 days of exposure.

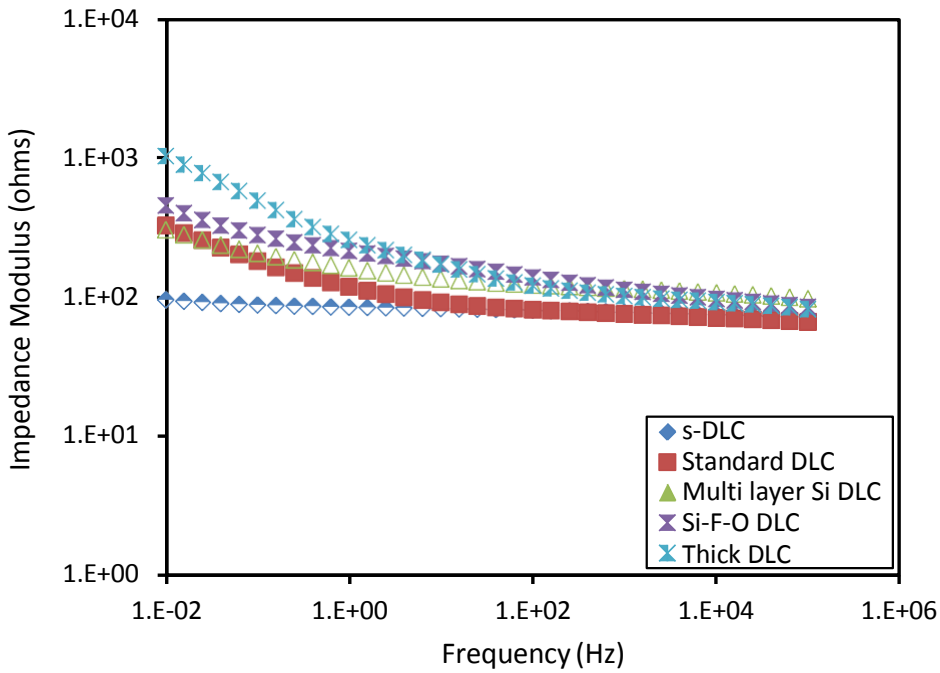

FIGURE 34 Impedance values of the DLC coatings embedded in mortars containing 5% chloride by wt. of mortar (batch 5) obtained after 86 days of exposure.

Visual Inspection

At the end of 140-day exposure, the mortar specimens were cut open and broken to retrieve the rebars for visual inspection. Figures 35–39 display the typical appearance of the coated rebars after exposure. For the mortars without added chlorides, no corrosion products were noted along the length in any of the coatings tested. As the chloride concentration increased, corrosion areas were recorded in some coatings, consistent with the results obtained by linear polarization resistance and EIS measurements. Table 5 summarizes the results of the visual examination performed by the end of exposure.

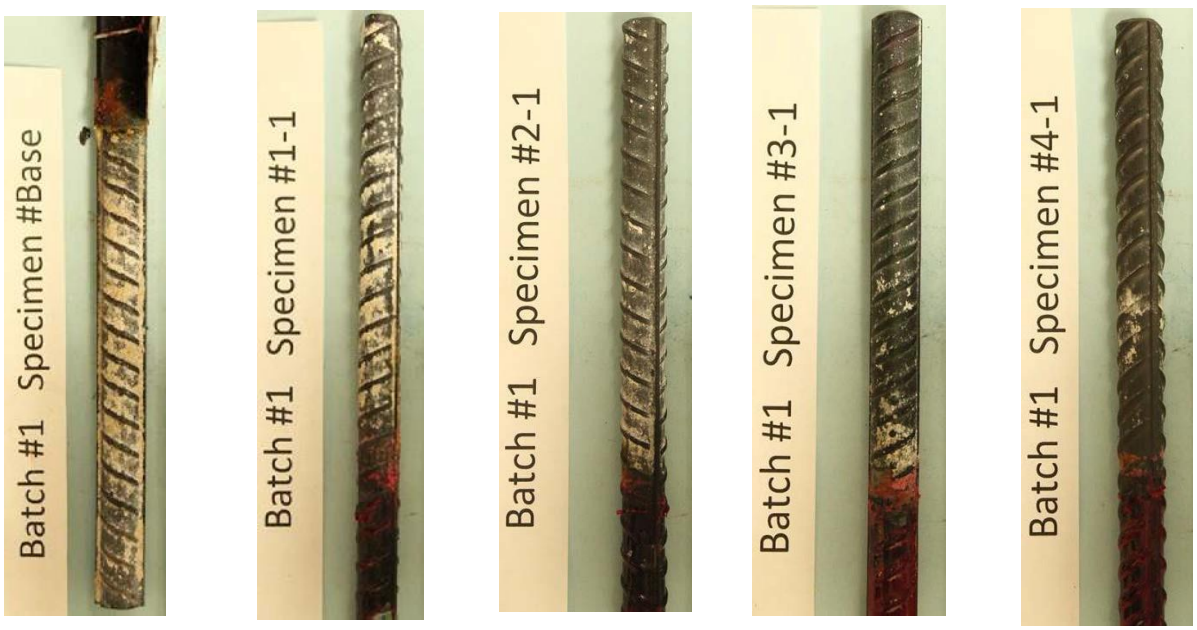

(A) (B) (C) (D) (E)

FIGURE 35 Autopsy of the DLC-coated rebars embedded in mortars without chlorides (batch 1): (A) s-DLC, (B) standard DLC, (C) multi-layer Si DLC, (D) Si-F-O DLC, and (E) thick DLC coatings.

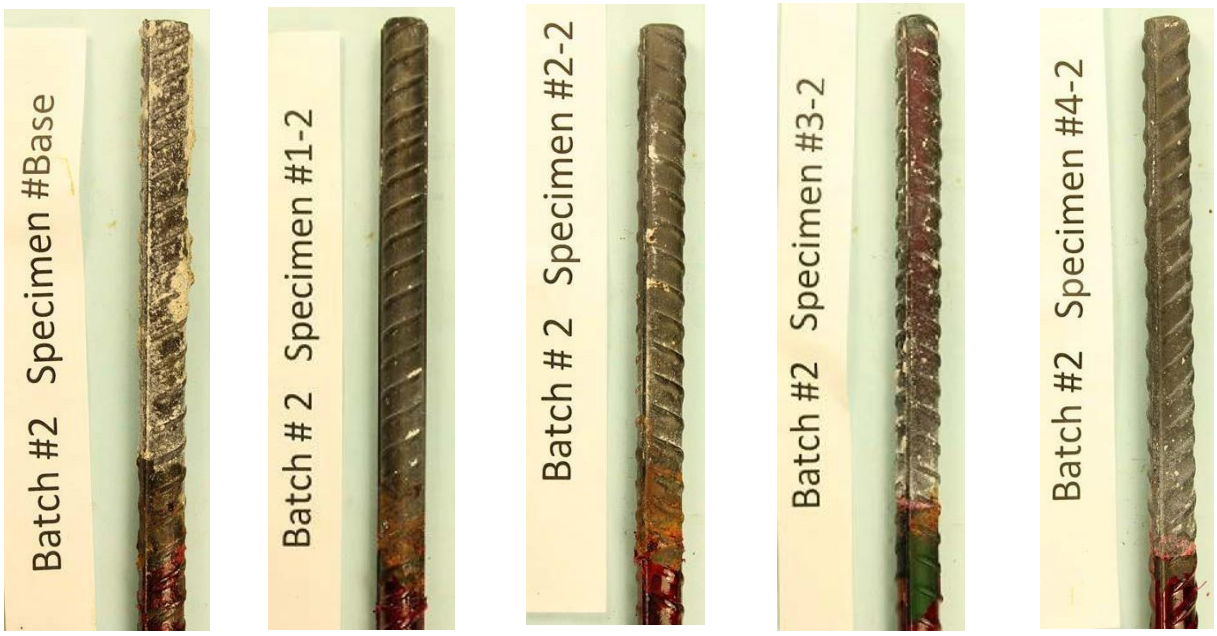

(A) (B) (C) (D) (E)

FIGURE 36 Autopsy of the DLC-coated rebars embedded in mortars containing 0.5% wt. chlorides (batch 2): (A) s-DLC, (B) standard DLC, (C) multi-layer Si DLC, (D) Si-F-O DLC, and (E) thick DLC coatings.

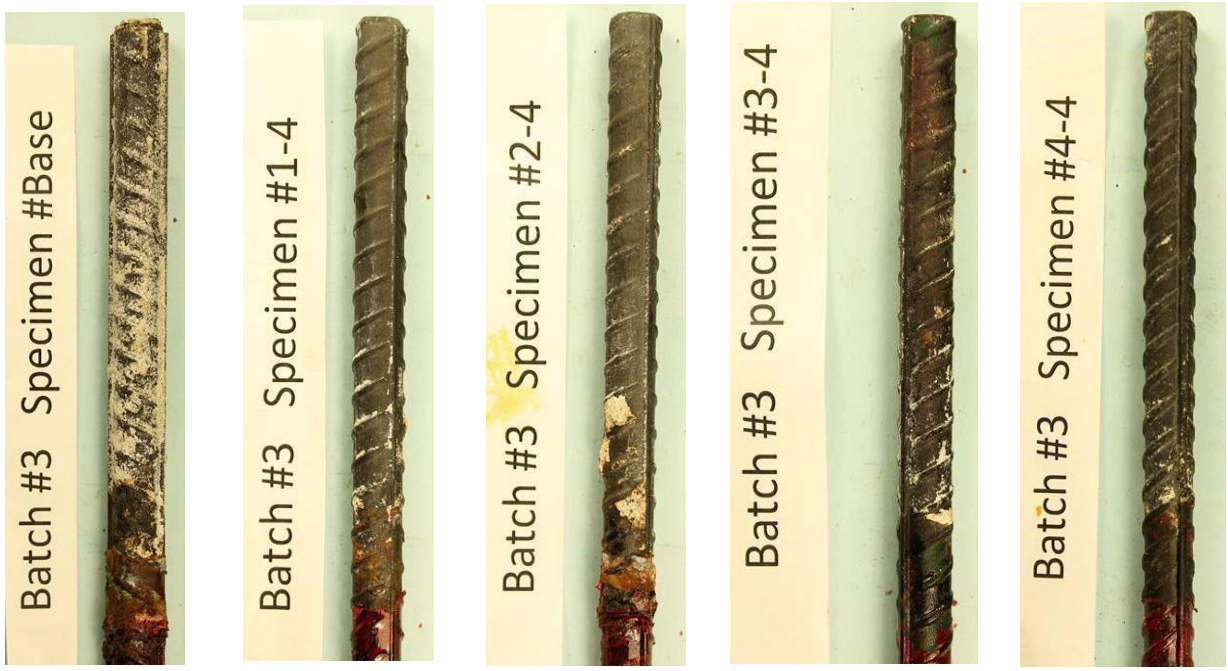

(A) (B) (C) (D) (E)

FIGURE 37 Autopsy of the DLC-coated rebars embedded in mortars containing 1% wt. chlorides (batch 3): (A) s-DLC, (B) standard DLC, (C) multi-layer Si DLC, (D) Si-F-O DLC, and (E) thick DLC coatings.

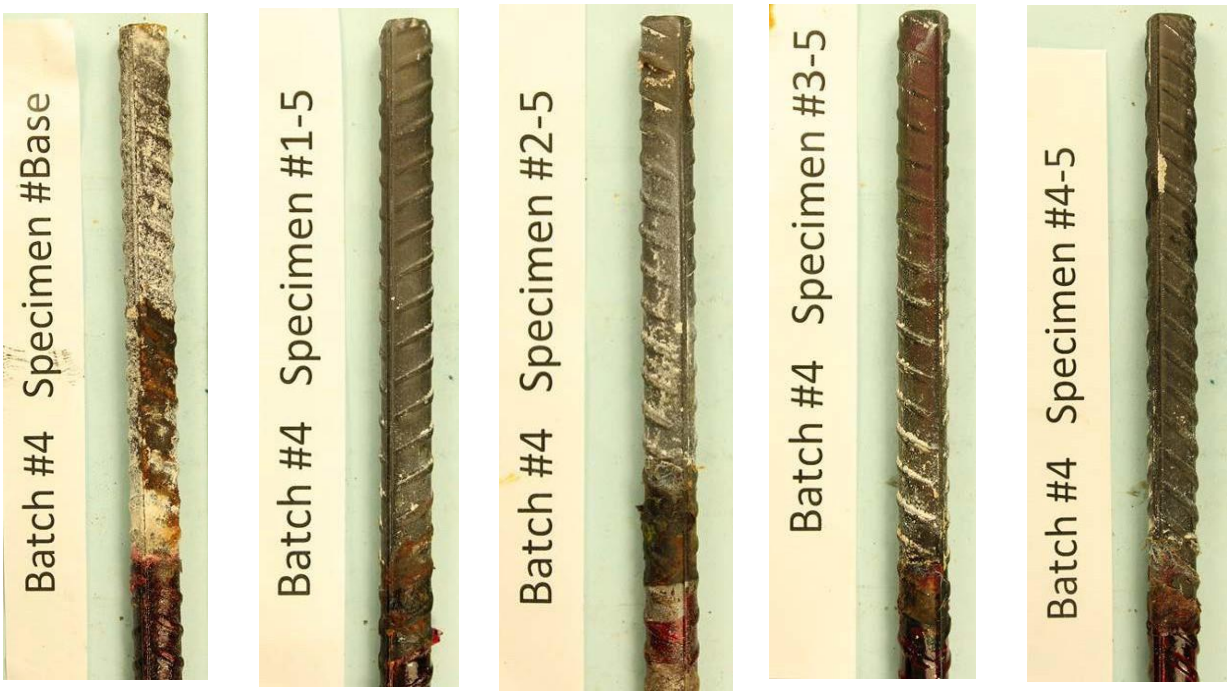

(A) (B) (C) (D) (E)

FIGURE 38 Autopsy of the DLC-coated rebars embedded in mortars containing 3% wt. chlorides (batch 4): s-DLC, (B) standard DLC, (C) multi-layer Si DLC, (D) Si-F-O DLC, and (E) thick DLC coatings.

(A) (B) (C) (D) (E)

FIGURE 39 Autopsy of the DLC-coated rebars embedded in mortars containing 5% wt. chlorides (batch 5): (A) s-DLC, (B) standard DLC, (C) multi-layer Si DLC, (D) Si-F-O DLC, and (E) thick DLC coatings.

TABLE 5
Summary of the results of the post visual examination of the coating rebars embedded in mortars containing varying amounts of admixed chlorides

<table>
<tr><th rowspan="2">Coating</th><th colspan="5">Mortars</th></tr>
<tr><th>[Cl$^-$] = 0%</th><th>[Cl$^-$] = 0.5%</th><th>[Cl$^-$] = 1%</th><th>[Cl$^-$] = 3%</th><th>[Cl$^-$] = 5%</th></tr>
<tr><td>s-DLC</td><td rowspan="4">No visible corrosion</td><td rowspan="2">Rust near top edge of mortar</td><td rowspan="2">Rust near top edge of mortar</td><td>Rust extending to center of rebar</td><td rowspan="3">Rust extending to center of rebar</td></tr>
<tr><td>Standard DLC</td><td rowspan="2">Rust near top edge of mortar</td></tr>
<tr><td>Multi-layer Si DLC</td></tr>
<tr><td>Si-F-O DLC</td><td rowspan="2">No visible corrosion</td><td rowspan="2">No visible corrosion</td><td rowspan="2">No visible corrosion</td><td>Minor corrosion spots</td></tr>
<tr><td>Thick DLC</td><td>No visible corrosion</td></tr>
</table>

CONCLUSIONS AND RECOMMENDATIONS

The results of this investigation indicate that the s-DLC coating may hold potential to be used as a protective coating to prevent corrosion of reinforcing steel in concrete. However, the current state of development suggests that improvements are needed to ensure that the coating is defect free. The key points of findings are summarized below:

1. Thick vacuum-deposited DLC coatings demonstrated an optimal performance in preventing corrosion of steel even at chloride concentration of 5% wt. of mortar. Corrosion rates for the thick DLC coatings were lower than 0.75 mils per year. This low corrosion rates values were in agreement with the absence of corrosion throughout the coated rebar surface.
2. Corrosion rust was noted in all the remaining DLC coatings with larger corrosion rates, more notable for the s-DLC coating. This suggests that coating breaks are present in the coating surface, reaching the underlying steel rebar.
3. To prevent formation of coating cracks, several modifications in the s-DLC coating were made. Changes in coating curing temperature and addition of binder agents were utilized with marginal success.

Future research is needed to further the development of the s-DLC coating to be usable as a cost-effective protective coating for reinforcing steel in concrete. While the mechanical properties of the s-DLC coating are excellent, its corrosion protective performance is still lacking. Southwest Research Institute (SwRI) will formalize teaming arrangements through negotiated business agreements to support technology integration and transition. SwRI has already engaged in discussions with small businesses regarding scale-up synthesis from the pilot synthesis to larger production (500–2,000 gallons) of s-DLC coatings. Additional potential technical transfer teaming partners include large chemical and coatings companies.

REFERENCES

1. Raupach, M. and P. Schiessl, *Construction and Building Materials*, Vol. 11, pp. 207–214 (1997).
2. Castellote, M., C. Andrade, and C. Alonso, *Corrosion Science*, Vol. 44, p. 2409 (2002).
3. Griffith, A. and H.M. Laylor, *Epoxy Coated Reinforcement Study*, Final Report, Project No. 527, Oregon Department of Transportation, Salem (1999).
4. Ramniceanu, A., R.E. Weyers, J.S. Riffle, and M.M. Sprinkel, "Parameters Governing Corrosion Protection Efficacy of Fusion-Bonded Epoxy Coatings on Reinforcing Bar," *ACI Materials Journal*, Vol. 105, p. 459 (2008).
5. Darwin, D. and J. Browning, "Concrete Bridge Conference," Paper No. 101, National Concrete Bridge Council, Skokie, Ill. (2008).
6. Lau, K. and A.A. Sagüés, "Corrosion of Epoxy- and Polymer/Zinc-Coated Rebar in Simulated Concrete Pore Solution," Paper No. 09207, Corrosion/2009, Atlanta, Ga. (2009).
7. Cui, F., Ph.D. Dissertation, University of South Florida, Tampa, (2003).
8. Visscher, G.T., D.C. Nesting, J.V. Badding, and P.A. Bianconni, *Science*, Vol. 260, pp. 1496–1499 (1993).
9. Katzenmeyer, *Journal of Nanomaterials*, 832327 (2009).
10. Bianconni, P.A., et al., *Journal of the American Chemical Society*, Vol. 126, pp. 3191–3202 (2004).
11. Papakonstantinou, P., J.F. Zhao, P. Lemoine, E.T. McAdams, and J.A. McLaughlin, "The Effects of Si Incorporation on the Electrochemical and Nanomechanical Properties of DLC Thin Films, *Diamond and Related Materials*, Vol. 11, pp. 1074–1080 (2002).
12. Liu, E. and H.W. Kwek, "Electrochemical Performance of Diamond-like Carbon Thin Films," *Thin Solid Films*, Vol. 516, pp. 5201–5205 (2008).
13. Vouagner, D., A.M. De Becdelievre, M. Keddam, and J.M. Mackowski, "The Electrochemical Behaviour in Acidic and Chloride Solutions of Amorphous Hydrogenated Carbon Thin Films Deposited on Single Crystal Germanium Slices (n-type) by Plasma Decomposition of Methane," *Corrosion Science*, Vol. 34, pp. 279–293 (1993).
14. Jellesen, M.S., T.L. Christiansen, L.R. Hilbert, and P. Møller, "Erosion-corrosion and Corrosion Properties of DLC Coated Low Temperature Gas-nitrided Austenitic Stainless Steel," *Wear*, Vol. 267, pp. 1709–1714 (2009).
15. Ellis, P.F., II and B.D. Chambers, "A Diamond-Like Carbon Pipe Lining Resistant to High Temperature and Pressure Carbon Dioxide/Hydrogen Sulfide Environments," In *NACE Corrosion*, Salt Lake City, Utah, pp. C2012–0001615 (2012).
16. Wei, R., Development of New Technologies and Practical Applications of Plasma Immersion Ion Deposition," *Surface and Coatings Technology*, Vol. 204, pp. 2869–2874 (2010).
17. Hatada, R. and K. Baba, "Preparation of Hydrophobic Diamond Like Carbon Films by Plasma Source Ion Implantation," *Nuclear Instruments and Methods in Physics Research Section B*, Vol., 148, pp. 655–658 (1999).
18. Method for Mechanical Mixing of Hydraulic Cement Pastes and Mortars of Plastic Consistency, ASTM C 305, American Society for Testing and Materials, Philadelphia, Pa., 1992.
19. Ma, M., G. Shi, and C.J. Xi, *Journal of Applied Polymer Science*, Vol. 89, pp. 16–23 (2003).
20. Hoey, G.R. and M. Cohen, "Corrosion of Anodically and Cathodically Polarized Magnesium in Aqueous Media," *Journal of the Electrochemical Society*, Vol. 105, No. 5, pp. 245–250 (1958).
21. Robertson, A., *Materials Science and Engineering R*, Vol. 37, pp. 129–281 (2002).
22. Zeng, A., et al., "EIS Capacitance Diagnosis of Nanoporosity Effect on the Corrosion Protection of DLC Films," *Diamond and Related Materials*, Vol. 11, pp. 160–168 (2002).
23. Pincheira, J., A.A. Aramayo, K. Kim, and D. Fratta, *Corrosion Protection Performance of Epoxy-Coated Reinforcing Bar*s, Final Report MN/RC 2008-47, Minnesota Department of Transportation, St. Paul (2008).
24. Lau, K., *Corrosion of Epoxy-coated Reinforcement in Marine Bridges with Locally Deficient Concrete*, Ph.D. Dissertation, University of South Florida, Tampa (2010).